

1 **Local artifacts in ice core methane records caused by**
2 **layered bubble trapping and in-situ production: a multi-**
3 **site investigation**

4

5 **Rachael H. Rhodes** ^{1*}, **Xavier Faïn** ², **Edward J. Brook** ¹, **Joseph R.**
6 **McConnell** ³, **Olivia J. Maselli** ³, **Michael Sigl** ^{3,4}, **Jon Edwards** ¹, **Christo**
7 **Buizert** ¹, **Thomas Blunier** ⁵, **Jérôme Chappellaz** ², **Johannes Freitag** ⁶

8

9 [1] {College of Earth, Ocean and Atmospheric Sciences, Oregon State University,
10 Corvallis OR, USA}

11 [2] {Université Grenoble Alpes/CNRS, Laboratoire de Glaciologie et Géophysique de
12 l'Environnement, Grenoble, France}

13 [3] {Division of Hydrologic Sciences, Desert Research Institute, Reno NV, USA}

14 [4] {Laboratory for Radiochemistry and Environmental Chemistry, Paul Scherrer Institut,
15 Villigen, Switzerland}

16 [5] {Centre for Ice and Climate, Niels Bohr Institute, University of Copenhagen,
17 Copenhagen Denmark}

18 [6] {Alfred Wegener Institute, Helmholtz Centre for Polar and Marine Research,
19 Bremerhaven, Germany}

20 [*] {now at Department of Earth Sciences, University of Cambridge, Cambridge, UK}

21

22 Correspondence to: R. H. Rhodes (rhr34@cam.ac.uk)

23

1 **Abstract**

2 Advances in trace gas analysis allow localised, non-atmospheric features to be resolved in
3 ice cores, superimposed on the coherent atmospheric signal. These high frequency
4 signals could not have survived the low-pass filter effect that firn diffusion exerts on the
5 atmospheric history and therefore do not result from changes in the atmospheric
6 composition at the ice sheet surface. Using continuous methane (CH₄) records obtained
7 from five polar ice cores, we characterize these non-atmospheric signals and explore their
8 origin. Isolated samples, enriched in CH₄ in the Tunu13 (Greenland) record are linked to
9 the presence of melt layers. Melting can enrich the methane concentration due to a
10 solubility effect, but we find that an additional in-situ process is required to generate the
11 full magnitude of these anomalies. Furthermore, in the all ice cores studied there is
12 evidence of reproducible, decimetre-scale CH₄ variability. Through a series of tests, we
13 demonstrate that this is an artifact of layered bubble trapping in a heterogeneous-density
14 firn column; we term this phenomenon ‘trapping signal’. The peak-to-peak amplitude of
15 the trapping signal is typically 5 ppb, but may exceed 40 ppb. Signal magnitude
16 increases with atmospheric CH₄ growth rate and seasonal density contrast, and decreases
17 with accumulation rate. Significant annual periodicity is present in the CH₄ variability of
18 two Greenland ice cores, suggesting that layered gas trapping at these sites is controlled
19 by regular, seasonal variations in the physical properties of the firn. Future analytical
20 campaigns should anticipate high frequency artifacts at high-melt ice core sites or during
21 time periods with high atmospheric CH₄ growth rate to avoid misinterpretation of such
22 features.

1 **1 Introduction**

2 Continuous measurement of ice core methane (CH₄) concentrations utilising laser
3 spectroscopy (Stowasser et al., 2012) is rapidly emerging as a powerful tool in
4 palaeoclimatology, producing highly detailed records of atmospheric methane for the
5 Last Glacial Period (Chappellaz et al., 2013; Rhodes et al., 2015) and Late Holocene
6 (Rhodes et al., 2013). The ability to expediently and precisely measure trace gases in ice
7 cores at centimetre-scale depth resolution also allows us to locally resolve novel, high
8 frequency signals that do not reflect past atmospheric conditions (Faïn et al., 2014;
9 Rhodes et al., 2013) but instead reveal new information about other processes that
10 influence trace gases in ice cores.

11 The processes of diffusive mixing and gradual bubble close-off, which occur in the firn
12 column, cumulatively act as a low-pass filter, removing high frequency atmospheric
13 signals, such as the CH₄ seasonal cycle (Schwander et al., 1993; Trudinger et al., 1997).
14 All polar ice cores therefore yield trace gas records that are smoothed versions of the
15 actual atmospheric history, with the degree of smoothing depending on site conditions,
16 particularly temperature and accumulation rate (Schwander et al., 1997). Although the
17 degree to which any atmospheric signal is damped by the firn is not always well
18 constrained in the past, it can be estimated (Rosen et al., 2014; Spahni et al., 2003).
19 Trace gas signals present at frequencies above those that could be preserved in the face of
20 the natural smoothing cannot represent atmospheric history. If they are present we must
21 assume that they are not related directly to the original atmospheric variation at the
22 surface of the ice sheet.

23 A previous study of Late Holocene Greenlandic ice (North Greenland Eemian Project
24 (NEEM)-2011-S1 ice core) (Rhodes et al., 2013) identified three categories of non-
25 atmospheric CH₄ signals:

26 1) *Infrequent, abrupt CH₄ spikes (20-100 cm depth interval, 35-80 ppb excess*
27 *CH₄) coincident with elevated concentrations of refractory black carbon and ammonium*
28 *(NH₄⁺), suggested to be linked to microbial in-situ production. Similar amplitude CH₄*
29 *anomalies, typically coeval with elevated NH₄⁺, were subsequently reported in Greenland*
30 *Ice Sheet Project 2 (GISP2) Holocene ice (Mitchell et al., 2013). The NEEM Community*

1 Members (2013) also implicated biological in-situ production in the much larger
2 amplitude (> 1000 ppb) CH₄ anomalies observed in NEEM ice dating from the last
3 interglacial (Eemian).

4 2) *CH₄ oscillations of > 100 ppb peak-to-peak amplitude through the lock-in zone.*

5 Following Etheridge et al. (1992), it was suggested that the CH₄ variability was related to
6 the mechanism of layered bubble trapping (Fig. 1). Briefly, according to this mechanism,
7 air bubbles in relatively dense layers close off earlier, trapping anomalously old air, and
8 air bubbles in less dense layers close off later, trapping relatively young air. Providing
9 that there is a sustained gradient of change in atmospheric methane across this time span,
10 the air bubbles in adjacent layers will contain different concentrations of methane.
11 Mitchell et al. (2015) quantified this phenomenon in samples from the lock-in zone of the
12 West Antarctic Ice Sheet (WAIS)-Divide ice core and developed a parameterisation for
13 layered bubble trapping in a firn densification model.

14 3) *Quasi-annual scale CH₄ oscillations of 24 ppb peak-to-peak amplitude in the*
15 *mature ice phase.* Such features had only been observed previously in mature ice at Law
16 Dome by Etheridge et al. (1992) who observed CH₄ variability consistent with younger
17 air being trapped in summer layers and older air trapped in winter layers. Although
18 Rhodes et al. (2013) hypothesized that they observed similar features, decimetre scale
19 CH₄ oscillations were observed throughout the NEEM-2011-S1 CH₄ record, not only
20 during periods of sustained change in atmospheric CH₄ concentration, questioning
21 whether all the resolved variability could be attributed to the layered bubble trapping
22 mechanism.

23 The findings summarised above generate many questions about what factors affect the
24 biological and/or physical mechanisms responsible for the non-atmospheric CH₄ signals
25 in polar glacial ice. For example, is the suspected in-situ production of CH₄ ubiquitous
26 across the Greenland ice sheet? Can similar anomalous signals be detected in Antarctic
27 ice that has a significantly lower impurity loading? How do site temperature,
28 accumulation rate and impurity load affect the high frequency CH₄ variability tentatively
29 linked to layered bubble close-off?

1 These questions are critically important because ice core trace gas records are integral to
2 palaeoclimatology, enabling us to investigate the relationship between atmospheric
3 greenhouse gases and climate prior to the late 20th century. Recent analytical advances in
4 both discrete (Mitchell et al., 2011) and continuous trace gas measurement techniques
5 (Rhodes et al., 2013; Stowasser et al., 2012) have increased data precision and resolution,
6 which is undoubtedly advantageous for palaeoclimate research, but also increases the
7 likelihood of resolving non-atmospheric signals. Avoiding misinterpretation of non-
8 atmospheric signals and therefore having confidence in the fidelity of the atmospheric
9 histories constructed from ice cores requires detailed knowledge of the physical and
10 biological processes that may locally affect trace gas records. This knowledge, acquired
11 from polar ice cores, could also provide hints about how to extract an atmospheric signal
12 from gas measurements performed on non-polar ice cores that are significantly affected by
13 such artifacts (e.g., Hou et al., 2013). Furthermore, by studying non-atmospheric artifacts
14 in ice core gas records we may learn about the physical mechanisms which trap air
15 bubbles in the firn enabling us to improve numerical model parameterisations used to
16 estimate the gas age-ice age difference and the smoothing effect of firn-based processes.
17 Additionally, it may be possible to glean information about biological activity in one of
18 the harshest biomes on Earth (Rohde et al., 2008).

19 This study examines Late Holocene CH₄ records with centimetre-scale resolution from
20 five polar ice cores with contrasting site characteristics (Table 1). Four of the cores are
21 from Greenland and one is from East Antarctica (Fig. S1). Accumulation rate and
22 temperature, the principal factors affecting firn densification rates, vary considerably
23 between the different cores. Concentrations of chemical impurities contained within the
24 ice can also vary by an order of magnitude (Table 1). Here we compare the ultra-high
25 resolution CH₄ records of the five different ice cores to show that the high frequency non-
26 atmospheric signals we previously observed in NEEM-2011-S1 ice are not unique to this
27 site. Furthermore, we demonstrate how several site characteristics influence the
28 frequency and magnitude of non-atmospheric signals.

29

1 **2 Methods**

2 **2.1 Sample description**

3 The ice core samples analysed in this study are listed in Table 1. Archived samples were
4 obtained from NEEM, D4 and North Greenland Ice Core Project (NGRIP). The NEEM
5 section was chosen to extend the existing NEEM-2011-S1 record further back in time.
6 The D4 record extends the NEEM-2011-S1 record forward in time and is from a warmer
7 Greenland site with twice the accumulation rate. The NGRIP samples are from two Late
8 Holocene depth intervals. A new ice core was retrieved from Tunu, NE Greenland,
9 where accumulation rates are about half those of NEEM or NGRIP. Hereafter the Tunu
10 core will be referred to as Tunu13 to avoid confusion with previous drilling projects.
11 Two Tunu13 cores were drilled: the first (Tunu13 Main) extended from the surface to
12 214 m depth and the second (Tunu13 B) from the surface to 140 m depth. The online gas
13 and chemistry records used in this study are predominantly from the Tunu13 Main core
14 with sections of Tunu13 B spliced in where poor core quality of Tunu13 Main core
15 caused deterioration of the records (Table S1). Prior to analysis, the Tunu13 cores were
16 logged at the National Ice Core Laboratory. Bottom depths of bubble-free layers were
17 recorded and top depths were recorded if the layer's width exceeded 4 mm. It was not
18 possible to discriminate visually between bubble-free layers that were melt layers and
19 those that were wind crusts (fine-grained, sintered layers thought to result from wind
20 action (Alley, 1988)). Both are likely to occur as Tunu is a windy site and our field team
21 found melt layers from the 2012 Greenland melt event. The B40 ice core was drilled
22 close to Kohnen Station, Dronning Maud Land, E Antarctica, by the Alfred Wegner
23 Institute and represents the coldest site with lowest impurity loading of the cores featured
24 in this study (Table 1).

25 **2.2 Analytical methods**

26 All the ice cores listed in Table 1 were analysed at the Desert Research Institute, Reno
27 NV, USA, using a continuous ice core melter system with online gas measurements
28 (Rhodes et al., 2015, 2013). Chemical concentrations in the liquid were measured
29 simultaneously, as described previously (McConnell et al., 2007, 2002).

1 An optical feedback cavity enhanced absorption spectrometer (SARA, developed at
2 Laboratoire Interdisciplinaire de Physique, University Grenoble Alpes, Grenoble, France)
3 (Morville et al., 2005) was used to analyse methane—the same instrument as used by
4 Rhodes et al. (2013) and Faïn et al. (2014). The system response time (time to reach 90%
5 of concentration step change (t_{90})) was 109 seconds, equivalent to 9.4–12.3 cm,
6 depending on the melt rate used for each ice core (Table S1). Methane data were
7 corrected for dissolution in the melted ice core sample following methods described
8 previously (Rhodes et al., 2013). Some system parameters, such as melt rate, varied
9 between ice cores to ensure the best compromise between measurement efficiency and
10 resolution (mainly in liquid phase) and different solubility corrections are used to account
11 for this (Table S1). Allan variance tests performed on measurements of synthetic sample
12 (standard gas mixed with degassed water) suggested an optimal integration time > 1000 s.
13 However, to maximise depth resolution we used an integration time of 5 s, for which
14 Allan variance tests suggest an internal precision of 1.7 ppb (2σ).

15 To limit entry of ambient air into the analytical system as breaks in the core were
16 encountered, ice was removed at any angled breaks to obtain a planar surface on which
17 the next ice stick could sit squarely. This resulted in some short sections of data loss.
18 Methane data were manually screened for spikes resulting from ambient air entry at the
19 melterhead (see also Sect. 3.2) because an automated screening algorithm proved too
20 aggressive, resulting in the removal of real variability, as confirmed by discrete CH_4
21 measurements.

22 Methane and chemistry data were mapped onto a depth scale using high resolution (0.1–
23 0.5 Hz acquisition rate) liquid conductivity data and time-depth relationships recorded by
24 system operators. A constant melt rate for each metre length of core is assumed. Depth
25 scale uncertainties are estimated to be ± 2 cm (2σ). The ice and gas age scales used for
26 each ice core are listed in Table 1.

27 For comparison, discrete samples from the Tunu13 ice core were analysed at Oregon
28 State University for methane concentration and total air content. Minor adjustments to
29 the methods of Mitchell et al. (2011) are described in the Supplementary Material.
30 Twenty-four ~ 15 cm depth sections were analysed at 6 cm resolution. External precision

1 of these data, estimated as pooled standard deviation of 34 duplicate (horizontally-
2 adjacent) sample sets, is 3.1 ppb for CH₄ and 0.002 cm³ STP g⁻¹ ice for total air content (1
3 σ).

4 **2.3 Firn air transport models**

5 We compare our empirical data to theoretical model predictions of CH₄ concentrations in
6 closed bubbles resulting from layered gas trapping produced by the Center for Ice and
7 Climate (CIC), Copenhagen, firn air transport model (Buizert et al., 2012). This model
8 includes parameterisation of stochastic gas trapping related to local density variability
9 (Mitchell et al., 2015). All experiments are run for the WAIS Divide ice core site
10 because high resolution local density data are available, as well as firn air sample data
11 needed to calibrate the diffusivity profile in the open pores. Model simulations are
12 performed at 1 cm vertical resolution to accurately capture the influence of layered
13 bubble trapping. Further details on modeling centimetre-scale air occlusion are provided
14 by Mitchell et al. (2015). The model simulations for the WAIS Divide ice core site can
15 be compared to Greenland ice core sites because the site conditions, particularly
16 temperature and accumulation rate, the principal factors to influence densification are
17 relatively similar (Table 1).

18 In addition, we use the OSU firn air transport model (Buizert et al., 2012), adapted for
19 palaeo-applications (Rosen et al., 2014), to estimate the smoothing effect that diffusion in
20 the firn has on the CH₄ atmospheric history at each ice core site (Fig. S2).

21

22 **3 Results and discussion**

23 **3.1 Integrity of the atmospheric CH₄ history from ice cores**

24 Multi-decadal scale atmospheric CH₄ variability, previously observed in Law Dome DSS
25 (MacFarling Meure et al., 2006), WAIS Divide (Mitchell et al., 2011), GISP2 (Mitchell et
26 al., 2013) and NEEM-2011-S1 (Rhodes et al., 2013), is faithfully replicated in all the ice
27 cores analysed in this study (Fig. 2). The multi-decadal signals recorded in each core
28 vary in amplitude because the original atmospheric signal has been smoothed to a
29 different extent at each site by firn-based processes (diffusive mixing and gradual bubble

1 occlusion). As expected, the low accumulation, cold, East Antarctic core B40 exhibits
2 the most extreme firn-based smoothing (orange line), and the Tunu13 record (green line)
3 shows significant signal damping compared to NGRIP (purple line) due to the lower
4 accumulation rates at Tunu. The estimated gas age distribution width (full width at half
5 maximum) at close-off depth for present-day conditions at each ice core site ranges from
6 14 yr at D4 to 65 yr at B40 (Table 1). Atmospheric signals of a shorter period than the
7 gas age distribution width are unlikely to be resolved with their full amplitude in the ice
8 core record.

9 **3.2 Potential in-situ CH₄ production and melt layers**

10 The continuous CH₄ records of all the ice cores analysed contained a high frequency
11 component superimposed on the coherent atmospheric signals shown in figure 2. For this
12 study it was particularly challenging to confidently distinguish between isolated
13 anomalously high CH₄ spikes present in-situ and those resulting from contamination by
14 ambient air. Forest fire haze over Reno during the analytical campaign meant that it was
15 not possible to rely on the absence of a carbon monoxide (CO) signal as indicative of
16 ambient air entry, as has previously been the case (Rhodes et al., 2013). This problem
17 was compounded by poor core quality (high break density, Table S1) in some core
18 sections. However, in a limited number of cases, discussed below, we were able to
19 distinguish between ambient air contamination and in-situ CH₄ signals.

20 Discrete CH₄ measurements performed on Tunu13 ice provided useful information
21 concerning isolated in-situ CH₄ spikes. The CH₄ concentrations of 5 of the 146 discrete
22 samples analysed (Table 2) were anomalously high, between 15 and 80 ppb greater than
23 adjacent samples. The elevated CH₄ samples also had relatively low air content values of
24 0.0847–0.0970 cm³ STP/g ice compared to median of 0.1002 cm STP/g ice (Table 2),
25 negating the possibility of sample contamination by an ambient air leak during analysis.
26 The five anomalous samples were all located within 2.5 cm of bubble-free layers logged
27 during processing (Figs. 3A, 3F-H, Table S2). We therefore hypothesize that these
28 bubble-free layers are melt layers. Anomalously high CH₄ values in ice cores have been
29 linked to melt layers because a) the solubility of CH₄ in water is greater than that of bulk
30 air, and/or b) previous studies suggest a potential for CH₄ production by microbial

1 activity, via reaction pathways that are currently unknown (Campen et al., 2003; NEEM
2 community members, 2013).

3 The CH₄ concentration and air content of each of these discrete samples represent a
4 mixture of air from standard bubbly ice and air from a melt layer. Each discrete sample
5 typically spanned 6 cm of ice core depth and, by comparison, the melt layers in the
6 Tunu13 cores were very thin, typically spanning < 5 mm depth. Given that we know the
7 dimensions of each sample and the proportion of the sample volume occupied by the melt
8 layer, we can estimate the CH₄ concentration in the melt layer itself (Table 2). We
9 assume that the air content of each melt layer is $0.0095 \pm 0.0037 \text{ cm}^3 \text{ STP g}^{-1} \text{ ice}$ (1σ
10 uncertainty, $n = 12$), which is the value measured at Oregon State University on melt
11 layer samples (from the 2012 melt event) collected at Summit, Greenland. Estimated
12 melt layer CH₄ concentrations range from 1829 (+704/-310) ppb to 6355 (+3585/-1574)
13 ppb, equivalent to 2.5–8.6 fold the atmospheric CH₄ concentrations at the time of melt
14 layer formation (Table 2). We then calculate the predicted CH₄ concentration of the melt
15 layers if dissolution of CH₄ from the atmosphere in liquid water reached equilibrium
16 (Table 2). Methane becomes relatively enriched in liquid water that is in equilibrium
17 with the atmosphere because methane is more soluble than nitrogen (Sander, 2015). The
18 predicted equilibrium CH₄ concentrations are all significantly lower than our estimated
19 melt layer concentrations, suggesting that another process, in addition to dissolution,
20 must contribute to the enrichment of CH₄ in melt layers. Our findings therefore support
21 those of the NEEM Community Members (2013), who found elevated CH₄
22 concentrations in excess of Henry's Law predictions across a melt layer in the Dye-3
23 (Greenland) ice core, and also those of Campen et al. (2003), who measured anomalously
24 high CH₄ values that could not be explained by dissolution effects alone. We note that in
25 this study we had to infer the CH₄ concentration of the melt layer because we were not
26 able to obtain a sample of pure melt layer, and the CH₄ values we estimate are relatively
27 uncertain.

28 In light of this apparent link between anomalously high CH₄ concentrations and melt
29 layers in Tunu13 ice, we re-examined the continuous CH₄ data and identified a further 14
30 bubble-free layers, coincident in depth with anomalous CH₄ spikes, that we assume are

1 melt layers (Table S2). The onset of these events can be extremely abrupt, making them
2 appear similar to ambient air contamination. 12 bubble-free layer depths had no
3 continuous CH₄ data, usually because data had been removed due to mixing with
4 standard at start/end of a run or because the ice had been removed across a badly-shaped
5 break. The CH₄ record at a further 20 bubble-free layer depths was affected by ambient
6 air contamination. There are also 78 bubble-free layer depths for which the CH₄ record
7 appears anomaly-free, suggesting that many of these observed bubble-free layers could
8 be wind crusts, not melt layers (Orsi et al., 2015). Alternatively, many of these bubble-
9 free layers did not span the entire horizontal area of the 10 cm diameter core and may
10 have not have been included in the 3.4 x 3.4 cm melter stick cut from the core.

11 We investigated the chemical composition (nitrate, refractory black carbon and
12 ammonium concentrations) of the suspected-melt layers with anomalously high CH₄,
13 because these chemical species were associated with isolated CH₄ spikes in the NEEM-
14 S1-2011 ice core (Rhodes et al., 2013) and GISP2 ice core ((Mitchell et al., 2013)
15 ammonium only). In the Tunu13 record, there was no significant difference between
16 chemical concentrations at depths coincident with anomalously high CH₄ linked to melt
17 layers and chemical concentrations at other depths (Fig. S3).

18 **3.3 Lock-in-zone CH₄ variability**

19 Methane concentrations were measured continuously up-core into the lock-in zone for
20 three ice cores: D4, Tunu13 and B40. We observed a marked increase in the amplitude
21 of decimetre-scale variability and a gradual decrease in gas flow to the instrument
22 through the lock-in zone (Fig. S4), similar to results produced by continuous CH₄
23 analysis of the lock-in zones in NEEM-2011-S1 (Rhodes et al., 2013) and WAIS Divide
24 (WDC05A, Mitchell et al. (2015)) ice cores. The sharp increase in the amplitude of high
25 frequency variability by up to 10-fold makes the base of the lock-in zone (close-off
26 depth) easily recognisable in continuous CH₄ data. We estimate the close-off depth to be
27 82 m at D4, 73 m at Tunu13 and 95 m at B40, comparable to values from firn air field
28 campaigns at the latter two sites (Tunu13: Butler et al., 1999; B40: Weiler, 2008). The
29 D4 continuous CH₄ data appear to encompass the entire lock-in zone.

1 Initial examination suggests that the magnitude of lock-in zone CH₄ variability varies
2 significantly between cores (Fig. S4) but it is not possible to quantify the degree of
3 ambient air contamination influencing our lock-in zone measurements, either from
4 laboratory air (~1890 ppb) via inter-connected open porosity or from post-coring bubble
5 closure (Aydin et al., 2010). It is therefore difficult to quantify the influence of layered
6 bubble trapping on lock-in zone CH₄ variability. However, we have reason to believe
7 that the proportion of ambient laboratory air versus air from the closed porosity may be
8 low because continuous CH₄ measurements of WAIS Divide lock-in zone samples
9 conducted using the same analytical system were well replicated by discrete CH₄
10 measurements (see Mitchell et al. (2015) Fig. S5). Furthermore, Mitchell et al. (2015)
11 used $\delta^{15}\text{N}$ of N₂ data measured on the WAIS Divide lock-in zone samples to calculate the
12 proportion of air affected by post-coring bubble closure as $10.6 \pm 6.1\%$; this value should
13 be considered as an upper estimate as the core used in that study was stored for ~ 6 yr
14 prior to analysis.

15 **3.4 High frequency non-atmospheric signals in mature ice**

16 **3.4.1 Observations**

17 In the mature ice phase below the close-off depth we observe significant decimetre-scale
18 variability in the CH₄ records of every ice core analysed. In each case, it is impossible
19 that this high frequency signal could have existed in the atmosphere at the ice sheet
20 surface and survived the low-pass filter action of the firn—the gas age distribution widths
21 (Table 1) are greater than the approximate signal periods. We initially focus in detail on
22 only Tunu13 and B40 because these are the most complete records, with relatively little
23 ice removed prior to analysis and few ambient air entry problems, both factors linked to
24 the number of core breaks (Table S1).

25 A smoothing spline is subtracted from the CH₄ record of each site to effectively remove
26 the atmospheric signal (Fig. 3A&B, Tunu13 shown). The residual CH₄ record contains a
27 high frequency, non-atmospheric signal and analytical noise (Fig. 3B). The mean peak-
28 to-peak amplitude (see Supplementary Material) of the residual high frequency CH₄ in
29 the Tunu13 record from 987 to 1870 AD gas age is 5.3 ppb (median is 3.7 ppb) and
30 varies between 2 ppb and 42 ppb. Variability of similar peak-to-peak amplitude and

1 frequency observed along the NEEM ice core continuous CH₄ profile was attributed to
2 analytical system noise (Chappellaz et al., 2013). Here, we have confidence that we
3 capture a high frequency signal present above the analytical noise in some sections of the
4 record because discrete CH₄ measurements on the Tunu13 core conducted at 6 cm
5 resolution also show substantial variability within each 15 cm depth section. CH₄
6 concentrations in adjacent samples differ by up to 32 ppb, but more typically by 3.4 ppb,
7 and reproduce some of the decimetre-scale changes resolved by the continuous
8 measurements (Fig. 3C-E). CH₄ oscillations captured by the discrete measurements are
9 larger in amplitude than those in the continuous gas record because the continuous gas
10 analysis system causes more signal smoothing than the discrete analysis (Stowasser et al.,
11 2012) (Table S1, Fig S2). The 5.3 ppb mean peak-to-peak amplitude of this high
12 frequency non-atmospheric signal must therefore be a minimum estimate of the true
13 signal in the ice.

14 A high frequency, non-atmospheric signal in excess of analytical noise is also present in
15 sections of the B40 continuous CH₄ record and it is reproducible; we measured replicate
16 ice core sticks on different days and were able to resolve very similar decimeter-scale
17 features in ice samples from 114–120 m depth (Fig. 4). The sharp CH₄ troughs at 122.8,
18 122.6, 122.3, 121.3 and 120.2 m are particularly well replicated and highly unlikely to be
19 analytical artifacts. The mean peak-to-peak amplitude of the high frequency non-
20 atmospheric signal in this section of the B40 record is 5.4 ppb (median is 5.1 ppb).

21 **3.4.2 Evidence for layered bubble trapping**

22 Our results demonstrate that the quasi-annual variability previously observed in the ice
23 phase of the NEEM-2011-S1 core (Rhodes et al., 2013) is not unique to NEEM or to
24 Greenlandic ice. The question now is: what causes it? If it is an artifact of layered
25 bubble trapping, as speculated for NEEM-2011-S1, the observed decimetre-scale
26 variability should respond in a predictable way to several factors that vary over time and
27 between ice core sites. We therefore systematically examine our empirical data to assess
28 the influence of each factor and judge whether any relationship is consistent with the
29 mechanism of layered bubble trapping.

30 - *Atmospheric CH₄ growth rate*

1 Our conceptual model of layered bubble trapping predicts that the difference in CH₄
2 concentration between adjacent layers (ΔCH_4) should increase with the CH₄ concentration
3 gradient in the firn column, which is dictated by the atmospheric CH₄ growth rate (Fig.
4 1). We can clearly observe this relationship in the Tunu13 record; amplitudes of the
5 decimetre-scale CH₄ oscillations are greatest when the atmospheric CH₄ concentration
6 shows a sustained trend of increase or decrease, particularly during the steep post-
7 Industrial Revolution CH₄ rise and the growth and decay in atmospheric CH₄
8 concentrations associated with the prominent CH₄ oscillation centered on 1550 AD (Fig.
9 3B).

10 To explore this relationship quantitatively, we compare the CH₄ growth rate to the
11 standard deviation (σ) of the high frequency CH₄ residual (data minus spline, as Fig. 3B)
12 for moving windowed sections of the Tunu13 record. Windows are 40 yr in length and
13 are calculated every 10 yr interval. Strong linear relationships between CH₄ growth rate
14 and the magnitude of high frequency variability are revealed for atmospheric CH₄ growth
15 and decay rates $> 0.4 \text{ ppb yr}^{-1}$ (Fig. 5E). The gradients of the linear relationships are
16 similar in both cases (7–8 ppb $\sigma\text{-CH}_4/\text{ppb yr}^{-1}$ growth rate). At low growth rates (< 0.4
17 ppb yr^{-1}) $\sigma\text{-CH}_4$ values reflect the analytical precision of 1.7 ppb. The observation that $\sigma\text{-}$
18 CH₄ only increases beyond analytical noise at growth rate $> 0.4 \text{ ppb yr}^{-1}$ heavily
19 implicates the mechanism of layered bubble trapping as the cause of the high frequency
20 CH₄ signal because it requires sustained trend of change in atmospheric concentration to
21 produce CH₄ artifacts (Fig. 1). We therefore define high frequency non-atmospheric CH₄
22 variability in excess of analytical noise as “trapping signal”.

23 This analysis was repeated on the high frequency CH₄ residual records from other ice
24 cores: B40, NEEM-2011-S1, D4 and NGRIP (Fig. 5 A-D). For NGRIP, only data from
25 1050–1240 AD and 1774–1860 AD (gas age) were used, the latter with a 10 yr length
26 window to avoid data gaps. For NEEM-2011-S1, data from 1450–1840 AD were used.
27 Any 40 yr time window with a data gap > 5 yr duration was discarded from analysis. We
28 note that the CH₄ growth rate recorded in the ice core is not strictly equivalent to the
29 atmospheric growth rate because firn-based smoothing may have caused some damping
30 of the signal (Fig. 2). The B40 record is significantly affected by firn-based smoothing
31 (Fig. S2), which reduces the growth rate captured by the ice core archive. The B40

1 record is also severely impacted by system-based smoothing (Fig. S2), which damps the
2 trapping signal to within range of the analytical noise for much of the record, excepting
3 the section displayed in figure 4. The combination of these two effects destroys any
4 relationship between atmospheric growth rate and amplitude of the high frequency signal
5 (Fig. 5A). There is also little sign of a relationship between growth rate and σ -CH₄ in the
6 NEEM-2011-S1 data (Fig. 5B) and we speculate this is the result of a more aggressive
7 ambient air screening method applied by Rhodes et al. (2013) that may have removed real
8 variability.

9 Results are more encouraging for D4 and NGRIP as both sites exhibit linear relationships
10 between CH₄ growth rate and the trapping signal magnitude (Fig. 5C&D). Both negative
11 and positive growth rates at NGRIP exhibit the same gradient of change with σ -CH₄. The
12 consistency of results between sites is important for the identification of layered bubble
13 trapping as the mechanism behind the high frequency variability. Further support can be
14 drawn from the CIC firm air transport model, which predicts a linear relationship between
15 atmospheric growth rate and the CH₄ trapping signal magnitude at WAIS Divide (red
16 line, Fig. 5F). When the Tunu13, D4 and NGRIP data are all plotted on the same axes
17 with the WAIS Divide model simulation (Fig. 5F), the gradient of the modeled linear
18 relationship is within the range of gradients of our empirical data from 3 different
19 Greenland ice core sites. Clearly, the CH₄ trapping signal magnitude (σ -CH₄) does not
20 have the same sensitivity to growth rate at all ice core sites; another factor is influencing
21 CH₄ variability, as we explore below.

22 For completeness we note that physics tells us that there can still be a tiny layered bubble
23 trapping signal at zero growth rate due to the effect of gravity. As CH₄ is lighter than air,
24 gravity reduces the CH₄ concentration with depth relative to the concentration in the
25 atmosphere. Thus at zero growth rate there is still a CH₄ gradient in the firm that can
26 result in the generation of a trapping signal via layered gas occlusion. This also means
27 that at positive atmospheric growth rates, the gravitational gradient must be overcome in
28 order to generate CH₄ oscillations related to layering. This is why the modeled WAIS
29 Divide growth rate vs. σ -CH₄ plot intersects the x-axis at a slightly positive growth rate
30 and σ -CH₄ is predicted to be 0.11 ppb at zero growth rate (Fig. 5F). This effect is an
31 order of magnitude smaller than the analytical noise and is not detectable.

1 - *Accumulation rate*

2 At a constant atmospheric growth rate, the CH₄ trapping signal amplitude produced by
3 layered bubble trapping should be determined by the difference in age between the air
4 trapped relatively early compared to younger air trapped relatively late (t_2 minus t_1 on
5 Fig. 1). One factor that will affect how quickly an adjacent layer is closed off is
6 accumulation rate (A)—more new snow accumulation will cause layers to spend less time
7 in the firm column reducing the time interval over which layered bubble trapping can
8 occur. We test this hypothesis by comparing the CH₄ trapping signal magnitude in ice
9 cores with different accumulation rates (Fig. 6A&B). Comparison is performed for two
10 discrete time periods (gas age) for which we have good quality (continuous and above
11 analytical noise) CH₄ residual data from three cores, and we assume all three sites
12 experienced the same atmospheric growth rate. As expected, there is a significant
13 decrease in σ -CH₄ with increasing accumulation rate for the 1770–1900 AD time period
14 (Fig. 7B), but the 1490–1630 AD interval shows shows no trend (Fig. 6A).

15 However, if we adjust the σ -CH₄ values of each ice core to compensate for the
16 differences in the smoothing effect of the analytical system, the results from the two time
17 intervals become more consistent (Fig. 6C&D). To perform this adjustment, we assume
18 that the high frequency signal has an annual periodicity and consult the Bode plots
19 generated from switching the analytical system between two gas standards, to determine
20 what fraction of the original amplitude is retained by the system (Fig. S2). The nature of
21 this relationship differs between time slices considered. An inverse relationship between
22 σ -CH₄ and annual layer thickness is identifiable for the 1490–1630 AD interval and a
23 power law fit is applied, but a linear relationship would also be applicable here. A power
24 law relationship is identifiable between annual layer thickness and σ -CH₄ for the 1770–
25 1900 AD time period, which has the greatest range of annual layer thickness and σ -CH₄
26 values. These corrected data suggest that, at a fixed growth rate, an inverse relationship
27 exists between accumulation rate and the magnitude of CH₄ variability (σ -CH₄). This is
28 how we would expect CH₄ trapping signal to respond to accumulation rate.

29 CIC firm air transport model simulations for WAIS Divide exhibit a similar power law
30 relationship to the empirical data, whereby σ -CH₄ is proportional to $1/A^{1.47}$. The slope is

1 the result of two separate effects. First, increasing A decreases the time adjacent layers
2 spend in the firn column, which by itself should cause CH_4 trapping signal to scale as
3 $1/A$. Second, at increased A the advective gas transport in the open pores is enhanced,
4 and this reduces the CH_4 gradient down the firn column. If bubbles are then trapped over
5 the same depth range, the amplitude of CH_4 variability will be reduced, and this effect
6 appears to scale as $1/A^{0.47}$ in the firn model. An important caveat is that the model
7 assumes no change in the firn density profile with changing accumulation rate, which is
8 unrealistic. However, the model does appear to capture a response of CH_4 trapping signal
9 to accumulation rate that is roughly comparable to that observable in the real-world data.

10 - *Firn layering*

11 Another factor that should influence the amount of time that passes between early and
12 late bubble closure is the degree of contrast between the physical properties of firn in
13 adjacent layers. There is no doubt that the physical properties of firn ultimately control
14 when a bubble is occluded, or a layer is completely sealed off. The relative importance
15 of local density variability, firn microstructure, permeability and/or porosity in this
16 process is actively debated. The traditional interpretation of density as the principal
17 influence on bubble occlusion is being challenged (Gregory et al., 2014). However, we
18 concentrate on the potential influence of local density variability in this section.

19 The controls on density layering in the firn are poorly understood, but a recent study
20 suggests that variability near the firn-ice transition is higher at warmer, high
21 accumulation sites (Hörhold et al., 2011). It is difficult to test the effects of density
22 layering because we do not have the high resolution density information required to do
23 so. However, we can use the CIC firn air transport model, which utilises high resolution
24 density data for the WAIS Divide ice core, to make a prediction. In these simulations, we
25 define the density layering to be $\rho_{\text{layer}} = \rho - \langle \rho \rangle$ with the local firn densities (ρ) as given
26 by the high resolution measurements, and the bulk density ($\langle \rho \rangle$) as given by a spline fit
27 to those data. We then run the model several times with a density profile that equals $\rho =$
28 $\langle \rho \rangle + \alpha \rho_{\text{layer}}$. By varying the scaling parameter α between 0 and 1.6 we can effectively
29 control the magnitude of the firn density layering. As we would expect, no high
30 frequency CH_4 trapping signal is produced in the absence of density layering ($\alpha = 0$) (Fig.

1 S5). When the magnitudes of the local density anomalies are halved ($\alpha = 0.5$), the
2 trapping signal amplitude decreases slightly more than 2-fold from 7.3 ppb to 3.2 ppb.
3 This effect is minor compared to that of accumulation rate or atmospheric growth rate.
4 However, it may explain why interior Antarctic sites, like B40, which have less
5 pronounced seasonality in density at the firn-ice transition compared to coastal Antarctic
6 or Greenland locations (Hörhold et al., 2011) may show only a moderate trapping signal
7 despite the extremely low accumulation rates.

8 **3.5 Layered gas trapping mechanism**

9 **3.5.1 Spatial and temporal information**

10 Having established that the high frequency CH₄ signal we observe in all the ice cores in
11 this study shows characteristics consistent with the mechanism of layered gas trapping
12 (Fig. 1), we are able to discern aspects of this physical process.

13 First, the CH₄ trapping signal measured for the different ice core sites allows us to
14 estimate the age difference between the air samples trapped in adjacent layers (t_2 minus t_1
15 on Fig. 1). High frequency CH₄ residual data, corrected for system smoothing effects
16 (Sect. 3.4.2) from the 1810–1860 AD time interval, which has an atmospheric growth rate
17 of 1.5 ppb yr⁻¹ (in D4—the least susceptible record to firn-based smoothing of the
18 atmospheric signal), suggest a gas age difference between adjacent layers of 23 yr at
19 Tunu13, 2.4 yr at D4 and 5 yr at NGRIP. These values can be compared to previously
20 published estimates of 10 yr for WAIS Divide (Mitchell et al., 2015), 12 yr for NEEM-
21 2011-S1 (Rhodes et al., 2013) and 2 yr for Law Dome (Etheridge et al., 1992).
22 Unsurprisingly, the gas age difference between adjacent layers is greater at lower
23 accumulation sites. To negate the issue of smoothing associated with the analytical
24 system, we also consider Tunu13 discrete measurements, which show a maximum
25 oscillation of 32 ppb amplitude at an atmospheric growth rate of 1.5 ppb yr⁻¹ (Fig. 3C).
26 The age difference between layers in this case would be 21 yr, which is very close to the
27 estimate above.

28 Second, the frequency of CH₄ oscillations resulting from layered bubble trapping should
29 reflect the difference in depth, and therefore also ice age (not the age of the gas trapped
30 inside the bubbles, as discussed above) between adjacent firn layers where bubbles are

1 closed off at different times. To test this with our ice core data we perform multi-taper
2 method (MTM) spectral analysis of the Tunu13, D4, NGRIP and B40 CH₄ records (Fig.
3 7). Spectral analysis is performed in the ice age domain because we believe that physical
4 properties of the firn/ice are ultimately responsible for the high frequency artifacts
5 recorded in the gas phase at the same depth. Prior to analysis, the data in each 40 yr
6 window (as Sect. 3.4.2) are interpolated to an even ice age spacing that is twice the
7 median sample spacing and any windows containing data gaps > 2 yr are ignored. We
8 then average the MTM spectra produced to generate mean spectra for sections of the
9 record with relatively high or low growth rate, or in the case of D4, sections of the record
10 encompassing only mature ice or some firn.

11 Sections of the Tunu13 record with CH₄ growth rates > 0.4 ppb yr⁻¹ exhibit spectral peaks
12 at 1 yr period in the ice age domain and the averaged spectrum for growth rates > 0.4 ppb
13 yr⁻¹ has a significant 1 yr periodicity (95% confidence) (Fig. 7). By contrast, sections of
14 the Tunu13 record with growth rates < ± 0.4 ppb yr⁻¹ show no significant periodicity.
15 The high accumulation Greenland ice core D4 shows an annual periodicity in CH₄, but it
16 only becomes significant when data from the lock-in zone are included (Fig. 7). NGRIP
17 shows small spectral peaks at 1 yr period for 2 out of 4 time windows with growth rates >
18 0.2 ppb yr⁻¹ but the peak in the averaged spectrum is not significant (Fig. 7). Again,
19 NGRIP data sections with growth rates < 0.2 ppb yr⁻¹ exhibit no periodicity. No
20 significant periodicity is resolved in the B40 high frequency residual CH₄ record,
21 potentially because any annual signal has been removed by analytical system smoothing.

22 The significant annual periodicity resolved in the Tunu13 and D4 records during periods
23 of relatively high growth rates strongly suggests that the mechanism of layered bubble
24 trapping is linked to regular, seasonal variations in the physical properties of the firn
25 pack, over a wide range of Greenland ice core site conditions. The quasi-annual high
26 frequency signal observed in mature NEEM-2011-S1 ice (Rhodes et al., 2013) could also
27 be added to this list. We note that even if there is some ambient air contamination of D4
28 lock-in zone CH₄ measurements, the wavelength of the CH₄ oscillations in the lock-in
29 zone should reflect the depth spacing of alternating layers with contrasting ratios of open
30 to closed porosity, and therefore relatively more or less contamination (Fig. 7).

1 **3.5.2 Implications for bubble closure in the firn column**

2 The regular oscillations between relatively young and relatively old air trapped in the ice
3 core air bubbles suggest that the early-closure layers (p_h on Fig. 1) are not sealing layers
4 which prevent vertical diffusion. In other words, some degree of open
5 porosity/permeability must be maintained in these early-closure layers to allow relatively
6 young air to diffuse down through the firn pack towards the late-closure layers (p_l on Fig.
7 1). This movement could be via vertical cracks or channels of open porosity tracking
8 around isolated clusters of closed pores in the early-closure layers (Keegan et al., 2014).
9 Furthermore, our results suggest that this situation must be maintained for upwards of 20
10 yr at the Tunu13 site.

11 The onset of the lock-in or non-diffusive zone (Sowers et al., 1992) is commonly
12 believed to be linked to horizontally-expansive sealing layers. Field measurements of
13 firn air (air pumped from the open porosity in the firn) provide strong evidence for such
14 sealing layers by demonstrating a lack of vertical mixing within the lock-in zone. For
15 example, halocarbon tracers linked to anthropogenic industrial activity are effectively
16 absent in the lock-in zone firn air at many sites (Butler et al., 1999; Severinghaus et al.,
17 2010; Sturrock et al., 2002). To first order, the trapping signal we observe in the ice
18 cores therefore suggests that significant bubble closure in the early-closure layers must
19 occur above the lock-in depth, where vertical diffusion of the relatively young air
20 required to form the regular CH_4 oscillations is not impeded. However, we do not rule
21 out a contribution to the trapping signal from within the lock-in zone because a) some
22 vertical pore connectivity in the lock-in zone is required to explain firn air observations at
23 NEEM (Buizert et al., 2012) and b) air content of mature ice is not consistent with fully
24 sealing layers at the lock-in depth (Martinerie et al., 1992). Measurements of WAIS
25 Divide lock-in zone samples suggest that much of the trapping signal is inherited from
26 bubble trapping above the lock-in depth, below which the signal gradually becomes
27 muted as vertical gas mixing is limited (Mitchell et al., 2015).

28 Our results suggest that the variations in local density and/or other related physical
29 properties, such as open porosity or grain size (Gregory et al., 2014) maintain an imprint
30 of annual variability towards the base of the firn column that is strong enough to produce

1 regular layering in the firn, resulting in a CH₄ trapping signal with a significant annual
2 periodicity. It is still not clear precisely how and why layering in polar firn evolves with
3 depth and time in the way that it does. Hörhold et al. (2012) suggested that “impurities”
4 which exhibit an annual cycle in concentration may act to promote densification by
5 softening the impurity-rich winter firn layers. Hörhold et al. (2012) reported positive
6 correlations between soluble calcium (Ca²⁺) concentration and local density but their
7 choice of Ca²⁺ was not supported by any causal physical link between Ca²⁺ and
8 densification rate. Ensuing work suggested that chloride (Cl⁻) and fluoride (F⁻) were
9 more likely candidates to drive densification at NEEM (Fujita et al., 2014), drawing on
10 early experiments which detail how substitution of Cl⁻ and F⁻ ions into the ice lattice
11 promotes dislocations and causes a softening effect (Jones, 1967; Nakamura and Jones,
12 1970). A subsequent study confirms these ideas by demonstrating their application to the
13 Dome Fuji ice core (Fujita et al., 2016). It is important to note that Fujita et al. (2016,
14 2014) also invoke a second, independent process that contributes to densification which
15 involves textural effects and is related to depositional conditions.

16 Our data cannot resolve this issue, but we can use the chemical concentrations measured
17 as a proxy for local density, assuming that winter/spring chemical species like Ca and Cl
18 are enriched in the relatively dense layers. In the Tunu13 ice core, concentrations of Ca
19 and Cl show significant negative correlation ($p < 0.05$) with CH₄ anomalies when growth
20 rates are positive (Fig. 8). A similar relationship is observable for the short section of the
21 B40 core with significant CH₄ trapping signal, using Na in place of Cl in this instance
22 because it is easier to measure at very low concentrations (Fig. 4B). These observations
23 confirm the seasonality of layered gas trapping that we have assumed—Ca and Cl-rich,
24 dense, layers trap air earlier, preserving a relatively low CH₄ concentration when
25 atmospheric CH₄ is increasing, and vice versa. Correlation between impurity levels in the
26 ice and CH₄ anomalies does not signify a causal link between them. It makes sense that
27 the correlation between ice chemistry and CH₄ is stronger at high growth rates because
28 the trapping signal produced at these times has relatively a high amplitude and an annual
29 periodicity. What is more interesting is that the sign of the correlation coefficient
30 between Ca or Cl and the high frequency CH₄ signal switches when CH₄ growth rate is
31 negative rather than positive (Fig. 8). When atmospheric CH₄ is decreasing, a Ca-Cl-rich

1 layer that closes off early will trap air with a relatively high CH₄ concentration. This is
2 an important final piece of evidence to attribute the high frequency CH₄ signal in ice
3 cores to layered bubble trapping.

4

5 **4 Summary**

6 **4.1 Methane artifacts related to melt layers**

7 We have demonstrated that narrow, isolated peaks in CH₄ concentration in the Tunu13 ice
8 core record are located at depths coincident with bubble-free layers assumed to be melt
9 layers. CH₄ measurements on discrete ice samples enabled us to confidently link melt
10 layers and CH₄ enrichment, circumventing the complication of potential ambient air
11 contamination from the continuous-flow system. These findings contrast with our
12 previous study (Rhodes et al., 2013), in which we found no melt layers associated with
13 anomalous CH₄ signals in the NEEM-2011-S1 core, but are in agreement with published
14 data showing trace gas enrichment across melt layers in the Dye 3 (Greenland) ice core
15 (NEEM community members, 2013; Neftel et al., 1983). Furthermore, we confirm this
16 and earlier work (Campen et al., 2003; NEEM community members, 2013) suggesting
17 that dissolution of CH₄ in the liquid phase cannot account for the full magnitude of CH₄
18 enrichment in melt layers, suggesting, but not proving, that biological activity may be in
19 part responsible for the observed CH₄ enrichment. Additionally, we find no significant
20 relationships between the anomalously high CH₄ levels at melt layer depths and
21 concentrations of chemical species (NH₄⁺, rBC or NO₃⁻) present in the ice phase of the
22 Tunu13 ice core.

23 In the absence of a systematic, reliable methodology to confidently distinguish between
24 elevated in-situ CH₄ signals and ambient air contamination, this study can only contribute
25 limited information regarding the potential for biological in-situ production of methane in
26 polar ice. The implications of biological in-situ production in polar ice are so far-
27 reaching (Priscu and Hand, 2010) that it deserves further investigation by a dedicated
28 multi-disciplinary project. Continuous trace gas analysis is an effective tool for screening
29 cores to identify depth ranges with interesting signals but further analysis including
30 δ¹³CH₄, organic species and meticulous microbiological characterisation are needed.

1 **4.2 Methane artifacts resulting from layered bubble trapping**

2 This study uses high resolution continuous CH₄ data from five Late Holocene ice cores to
3 demonstrate that layered bubble trapping causes high frequency (decimetre-scale)
4 oscillations in the CH₄ record of mature ice from both Antarctica and Greenland when
5 there is a sustained positive or negative trend in atmospheric growth rate. This trapping
6 signal has been reproduced by discrete and continuous CH₄ measurements and cannot
7 reflect atmospheric history because firn-based smoothing processes would have removed
8 it.

9 Using empirical data supported by firn air transport model simulations we demonstrate
10 that the CH₄ trapping signal responds in predictable ways to atmospheric growth rate and
11 site specific factors, particularly accumulation rate. The amplitude of the CH₄ trapping
12 signal increases with atmospheric growth rate and seasonal density contrasts, and
13 decreases with accumulation rate. The layered bubble trapping signal in two Greenland
14 ice core records has a significant annual periodicity, demonstrating that the seasonal
15 contrasts in firn physical properties which develop above the firn-ice transition are
16 regular and uniform enough to generate periodic CH₄ artifacts.

17 **5 Implications**

18 **5.1.1 For future ice core trace gas analysis**

- 19 • As resolution and precision of analytical techniques improve, analysts need to be
20 aware that non-atmospheric, high frequency signals are present in ice core trace gas
21 records resulting from enrichment associated with melt layers and variability related
22 to layered bubble trapping during.
- 23 • Careful choices regarding discrete sample size and dimension, and post-processing of
24 continuous data sets are required to avoid misinterpretation. Analysts should
25 integrate trace gas data over multiple annual layers to smooth out the trapping signal,
26 paying particular attention to time periods of relatively high atmospheric CH₄ growth
27 rate. Isolated anomalous CH₄ signals should be anticipated at sites where surface
28 melt is possible. These considerations are especially relevant for studies of the inter-

1 polar gradient (e.g., Mitchell et al., 2013) because the absolute concentrations are so
2 important to the conclusions reached.

- 3 • The magnitude of CH₄ trapping signal within an ice core record or in a time slice can
4 be predicted using a firm air transport model adapted for the purpose (Mitchell et al.,
5 2015), provided information about the local density variability at the site is known.
6 Density information from the firm could plausibly be extrapolated to Holocene ice but
7 not to ice from widely different climatic conditions. If variability in chemical
8 concentrations or impurities recorded in the ice phase could somehow be interpreted
9 as a proxy for local density variability, this could help to inform modeling efforts.
10 This study presents only an incremental step towards utilising chemistry records in
11 this way.

12 **5.1.2 For our understanding of gas trapping**

- 13 • Our empirical data demonstrate that layered gas trapping is driven by highly regular
14 (seasonal) variations in the physical properties of layered firm, as suggested by
15 Martinerie et al. (1992). Whether local density or some other closely-related property
16 is primarily responsible for driving this seasonal variability in bubble occlusion is not
17 clear.
- 18 • The regular CH₄ oscillations of the trapping signal indicate that significant bubble
19 closure must occur in the early-closure layers above the lock-in depth. Vertical
20 diffusion through early-closure layers must be maintained for several years (our
21 observations suggest up to 20 yr) to allow relatively young air to become trapped in
22 late-closure layers below.
- 23 • Despite the many bubble-free layers observed in the Tunu13 ice core, we do not find
24 evidence of fully ‘sealing layers’ above the lock-in zone—there is no major departure
25 from the relationship between trapping signal and linear atmospheric growth rate
26 (Fig. 5). Such a layer has only been observed previously in the Law Dome DE08-2
27 ice core; this thick melt layer caused an 80% reduction in gas diffusion (Trudinger et
28 al., 1997). A recent examination of bubble-free layers in the WAIS Divide core also
29 found no evidence for significant impact on gas transport (Orsi et al., 2015).

- 1 • The layered bubble trapping process has the effect of broadening the *modelled* gas
2 age distribution of the air in ice cores, relative to a model scenario without layered
3 bubble trapping but the same prescribed firn air diffusivity profile. Age distributions
4 in realistic models of non-layered firn compared to layered firn that capture the effect
5 of layering on the diffusivity have yet to be studied, as far as we are aware. However,
6 in nature, the presence of firn layering presumably leads to the formation of a lock-in
7 zone, which causes a narrowing of the gas age distribution by limiting vertical
8 diffusion. The net effect of firn layering is therefore likely to be a reduction in the
9 width of the gas age distribution of air trapped in ice cores (Mitchell et al., 2015).

10 An open question generated by this study is: Why do the high frequency oscillations in
11 CH₄ concentration increase sharply in amplitude across the transition from mature ice
12 into the lock-in zone (Sect. 3.3)? The findings of Mitchell et al. (2015) suggest that
13 contamination from ambient air is relatively low in continuous data from the lock-in
14 zone, not enough to account for the 10-fold amplitude increase. So, if CH₄ variability in
15 the lock-in zone and in the mature ice phase are both related to layered bubble trapping,
16 what causes the discontinuity? Could it be that drilling and cutting the ice samples
17 inherently influences the observations by re-opening centimetre-scale pore clusters that
18 were already closed off from the atmosphere? It may be that the only way to resolve this
19 question is to devise a way to eliminate firn air alteration caused by both ambient air
20 contamination and the re-opening of pores, perhaps by analysing trace gases across the
21 lock-in zone to mature ice transition in-situ.

22

23 **Acknowledgements**

24 This work was supported by US National Science Foundation (NSF) grants 1204172,
25 0944552, 1204176 and 0909541 and NSF Partnerships in International Research and
26 Education (PIRE) Grant 0968391. This work was additionally supported by the French
27 ANR program RPD COCLICO (ANR-10-RPDOC-002-01) and received funding from
28 the European Research Council under the European Community's Seventh Framework
29 Program FP7/2007-2013 Grant Agreement #291062 (project ICE&LASERS). Jeffrey
30 Severinghaus and David Etheridge provided insightful reviews that improved this

1 manuscript. We thank Nathan Chellman, Daniel Pasteris, Larry Layman and Amber
2 Zandanel for laboratory assistance, Nicole Rocco for Summit melt layer measurements,
3 and Julia Rosen for use of OSU firm model. We are very grateful to Beth “Bella”
4 Bergeron for her valuable expertise, leadership and hard work drilling the Tunu13 cores.
5 Our field team received valuable assistance from CHM2HILL and Ken Borek Air. The
6 NEEM project is directed by the Centre for Ice and Climate at the Niels Bohr Institute,
7 Copenhagen and the US NSF OPP. It is supported by funding agencies and institutions in
8 Belgium (FNRS-CFB and FWO), Canada (NRCan/GSC), China (CAS), Denmark
9 (FIST), France (IPEV, CNRS/INSU, CEA and ANR), Germany (AWI), Iceland (RannIs),
10 Japan (NIPR), Korea (KOPRI), The Netherlands (NWO/ALW), Sweden (VR),
11 Switzerland (SNF), United Kingdom (NERC) and the USA (US NSF, OPP). We are
12 grateful to the North Greenland Ice Core Project (NGRIP) for providing samples.

1 **References**

- 2 Alley, B., 1988. Concerning the deposition and diagenesis of strata in polar firn. *J.*
3 *Glaciol.* 34, 283–290.
- 4 Aydin, M., Montzka, S.A., Battle, M.O., Williams, M.B., De Bruyn, W.J., Butler, J.H.,
5 Verhulst, K.R., Tatum, C., Gun, B.K., Plotkin, D.A., Hall, B.D., Saltzman, E.S.,
6 2010. Post-coring entrapment of modern air in some shallow ice cores collected
7 near the firn-ice transition: evidence from CFC-12 measurements in Antarctic firn
8 air and ice cores. *Atmos Chem Phys* 10, 5135–5144. doi:10.5194/acp-10-5135-
9 2010
- 10 Buizert, C., Martinerie, P., Petrenko, V.V., Severinghaus, J.P., Trudinger, C.M., Witrant,
11 E., Rosen, J.L., Orsi, A.J., Rubino, M., Etheridge, D.M., Steele, L.P., Hogan, C.,
12 Laube, J.C., Sturges, W.T., Levchenko, V.A., Smith, A.M., Levin, I., Conway,
13 T.J., Dlugokencky, E.J., Lang, P.M., Kawamura, K., Jenk, T.M., White, J.W.C.,
14 Sowers, T., Schwander, J., Blunier, T., 2014. Corrigendum to ‘‘Gas transport in
15 firn: multiple-tracer characterisation and model intercomparison for NEEM,
16 Northern Greenland’’ published in *Atmos. Chem. Phys.*, 12, 4259–4277, 2012.
17 *Atmos Chem Phys* 14, 3571–3572. doi:10.5194/acp-14-3571-2014
- 18 Buizert, C., Martinerie, P., Petrenko, V.V., Severinghaus, J.P., Trudinger, C.M., Witrant,
19 E., Rosen, J.L., Orsi, A.J., Rubino, M., Etheridge, D.M., Steele, L.P., Hogan, C.,
20 Laube, J.C., Sturges, W.T., Levchenko, V.A., Smith, A.M., Levin, I., Conway,
21 T.J., Dlugokencky, E.J., Lang, P.M., Kawamura, K., Jenk, T.M., White, J.W.C.,
22 Sowers, T., Schwander, J., Blunier, T., 2012. Gas transport in firn: multiple-tracer
23 characterisation and model intercomparison for NEEM, Northern Greenland.
24 *Atmospheric Chem. Phys.* 12, 4259–4277. doi:10.5194/acp-12-4259-2012
- 25 Butler, J.H., Battle, M., Bender, M.L., Montzka, S.A., Clarke, A.D., Saltzman, E.S.,
26 Sucher, C.M., Severinghaus, J.P., Elkins, J.W., 1999. A record of atmospheric
27 halocarbons during the twentieth century from polar firn air. *Nature* 399, 749–
28 755. doi:10.1038/21586
- 29 Campen, R.K., Sowers, T., Alley, R.B., 2003. Evidence of microbial consortia
30 metabolizing within a low-latitude mountain glacier. *Geology* 31, 231–234.
31 doi:10.1130/0091-7613
- 32 Chappellaz, J., Stowasser, C., Blunier, T., Baslev-Clausen, D., Brook, E.J., Dallmayr, R.,
33 Faïn, X., Lee, J.E., Mitchell, L.E., Pascual, O., Romanini, D., Rosen, J.,
34 Schüpbach, S., 2013. High-resolution glacial and deglacial record of atmospheric
35 methane by continuous-flow and laser spectrometer analysis along the NEEM ice
36 core. *Clim Past* 9, 2579–2593. doi:10.5194/cp-9-2579-2013
- 37 Etheridge, D., Pearman, G.I., Fraser, P.J., 1992. Changes in tropospheric methane
38 between 1841 and 1978 from a high accumulation-rate Antarctic ice core. *Tellus*
39 44B, 282–294.
- 40 Faïn, X., Chappellaz, J., Rhodes, R.H., Stowasser, C., Blunier, T., McConnell, J.R.,
41 Brook, E.J., Preunkert, S., Legrand, M., Debois, T., Romanini, D., 2014. High
42 resolution measurements of carbon monoxide along a late Holocene Greenland
43 ice core: evidence for in situ production. *Clim Past* 10, 987–1000. doi:10.5194/cp-
44 10-987-2014

- 1 Fujita, S., Goto-Azuma, K., Hirabayashi, M., Hori, A., Iizuka, Y., Motizuki, Y.,
2 Motoyama, H., Takahashi, K., 2016. Densification of layered firn in the ice sheet
3 at Dome Fuji, Antarctica. *J. Glaciol. FirstView*, 1–21. doi:10.1017/jog.2016.16
- 4 Fujita, S., Hirabayashi, M., Goto-Azuma, K., Dallmayr, R., Satow, K., Zheng, J., Dahl-
5 Jensen, D., 2014. Densification of layered firn of the ice sheet at NEEM,
6 Greenland. *J. Glaciol.* 60, 905–921. doi:10.3189/2014JoG14J006
- 7 Gregory, S.A., Albert, M.R., Baker, I., 2014. Impact of physical properties and
8 accumulation rate on pore close-off in layered firn. *The Cryosphere* 8, 91–105.
9 doi:10.5194/tc-8-91-2014
- 10 Hörhold, M.W., Kipfstuhl, S., Wilhelms, F., Freitag, J., Frenzel, A., 2011. The
11 densification of layered polar firn. *J. Geophys. Res.* 116, F01001.
12 doi:10.1029/2009jf001630
- 13 Hörhold, M.W., Laepple, T., Freitag, J., Bigler, M., Fischer, H., Kipfstuhl, S., 2012. On
14 the impact of impurities on the densification of polar firn. *Earth Planet. Sci. Lett.*
15 325–326, 93–99. doi:10.1016/j.epsl.2011.12.022
- 16 Hou, S., Chappellaz, J., Raynaud, D., Masson-Delmotte, V., Jouzel, J., Bousquet, P.,
17 Hauglustaine, D., 2013. A new Himalayan ice core CH₄ record: possible hints at
18 the preindustrial latitudinal gradient. *Clim. Past* 9, 2549–2554. doi:10.5194/cp-9-
19 2549-2013
- 20 Jones, S.J., 1967. Softening of ice crystals by dissolved fluoride ions. *Phys. Lett. A* 25,
21 366–367. doi:10.1016/0375-9601(67)90702-5
- 22 Keegan, K., Albert, M.R., Baker, I., 2014. The impact of ice layers on gas transport
23 through firn at the North Greenland Eemian Ice Drilling (NEEM) site, Greenland.
24 *The Cryosphere* 8, 1801–1806. doi:10.5194/tc-8-1801-2014
- 25 Klein, K., 2014. Variability in dry Antarctic firn—Investigations on spatially distributed
26 snow and firn samples from Dronning Maud Land, Antarctica. PhD thesis,
27 University of Bremen, Bremen, Germany.
- 28 MacFarling Meure, C., Etheridge, D., Trudinger, C., Steele, P., Langenfelds, R., van
29 Ommen, T., Smith, A., Elkins, J., 2006. Law Dome CO₂, CH₄ and N₂O ice core
30 records extended to 2000 years BP. *Geophys. Res. Lett.* 33,
31 doi:10.1029/2006GL026152.
- 32 Martinerie, P., Raynaud, D., Etheridge, D.M., Barnola, J.-M., Mazaudier, D., 1992.
33 Physical and climatic parameters which influence the air content in polar ice.
34 *Earth Planet. Sci. Lett.* 112, 1–13. doi:10.1016/0012-821X(92)90002-D
- 35 McConnell, J.R., Aristarain, A.J., Banta, J.R., Edwards, P.R., Simões, J.C., 2007. 20th-
36 Century doubling in dust archived in an Antarctic Peninsula ice core parallels
37 climate change and desertification in South America. *Proc. Natl. Acad. Sci.* 104,
38 5743–5748.
- 39 McConnell, J.R., Lamorey, G.W., Lambert, S.W., Taylor, K.C., 2002. Continuous ice-
40 core chemical analyses using inductively coupled plasma mass spectrometry.
41 *Environ. Sci. Technol.* 36, 7–11. doi:10.1021/es011088z
- 42 Mitchell, L., Brook, E., Lee, J.E., Buizert, C., Sowers, T., 2013. Constraints on the Late
43 Holocene anthropogenic contribution to the atmospheric methane budget. *Science*
44 342, 964–966. doi:10.1126/science.1238920

- 1 Mitchell, L.E., Brook, E.J., Sowers, T., McConnell, J.R., Taylor, K., 2011. Multidecadal
2 variability of atmospheric methane, 1000-1800 C.E. *J. Geophys. Res.* 116,
3 doi:10.1029/2010JG001441. doi:10.1029/2010jg001441
- 4 Mitchell, L.E., Buizert, C., Brook, E.J., Breton, D.J., Fegyveresi, J., Baggenstos, D., Orsi,
5 A., Severinghaus, J., Alley, R.B., Albert, M., Rhodes, R.H., McConnell, J.R.,
6 Sigl, M., Maselli, O., Gregory, S., Ahn, J., 2015. Observing and modeling the
7 influence of layering on bubble trapping in polar firn. *J. Geophys. Res.*
8 *Atmospheres* 120, 2558–2574. doi:10.1002/2014JD022766
- 9 Morville, J., Kassi, S., Chenevier, M., Romanini, D., 2005. Fast, low-noise, mode-by-
10 mode, cavity-enhanced absorption spectroscopy by diode-laser self-locking. *Appl.*
11 *Phys. B Lasers Opt.* 80, 1027–1038.
- 12 Nakamura, T., Jones, S.J., 1970. Softening effect of dissolved hydrogen chloride in ice
13 crystals. *Scr. Metall.* 4, 123–126. doi:10.1016/0036-9748(70)90176-6
- 14 NEEM community members, 2013. Eemian interglacial reconstructed from a Greenland
15 folded ice core. *Nature* 493, 489–494.
- 16 Neftel, A., Oeschger, H., Schwander, J., Stauffer, B., 1983. Carbon dioxide concentration
17 in bubbles of natural cold ice. *J. Phys. Chem.* 87, 4116–4120.
18 doi:10.1021/j100244a025
- 19 NGRIP community members, 2004. High-resolution record of Northern Hemisphere
20 climate extending into the last interglacial period. *Nature* 431, 147–151.
- 21 Orsi, A.J., Kawamura, K., Fegyveresi, J.M., Headly, M.A., Alley, R.B., Severinghaus,
22 J.P., 2015. Differentiating bubble-free layers from melt layers in ice cores using
23 noble gases. *J. Glaciol.* 61, 585–594.
- 24 Priscu, J.C., Hand, K.P., 2010. Microbial habitability of icy worlds. *Microbe Mag. Am.*
25 *Soc. Microbiol.*
- 26 Rasmussen, S.O., Abbott, P.M., Blunier, T., Bourne, A.J., Brook, E., Buchardt, S.L.,
27 Buizert, C., Chappellaz, J., Clausen, H.B., Cook, E., Dahl-Jensen, D., Davies,
28 S.M., Guillevic, M., Kipfstuhl, S., Laepple, T., Seierstad, I.K., Severinghaus, J.P.,
29 Steffensen, J.P., Stowasser, C., Svensson, A., Vallelonga, P., Vinther, B.M.,
30 Wilhelms, F., Winstrup, M., 2013. A first chronology for the North Greenland
31 Eemian Ice Drilling (NEEM) ice core. *Clim Past* 9, 2713–2730. doi:10.5194/cp-9-
32 2713-2013
- 33 Rhodes, R.H., Brook, E.J., Chiang, J.C., Blunier, T., Maselli, O.J., McConnell, J.R.,
34 Romanini, D., Severinghaus, J.P., 2015. Enhanced tropical methane production in
35 response to iceberg discharge in the North Atlantic. *Science* 348, 1016–1019.
- 36 Rhodes, R.H., Faïn, X., Stowasser, C., Blunier, T., Chappellaz, J., McConnell, J.R.,
37 Romanini, D., Mitchell, L.E., Brook, E.J., 2013. Continuous methane
38 measurements from a late Holocene Greenland ice core: Atmospheric and in-situ
39 signals. *Earth Planet. Sci. Lett.* 368, 9–19. doi:10.1016/j.epsl.2013.02.034
- 40 Rohde, R.A., Price, P.B., Bay, R.C., Bramall, N.E., 2008. In situ microbial metabolism as
41 a cause of gas anomalies in ice. *Proc. Natl. Acad. Sci.* 105, 8667–8672.
42 doi:10.1073/pnas.0803763105
- 43 Rosen, J.L., Brook, E.J., Severinghaus, J.P., Blunier, T., Mitchell, L.E., Lee, J.E.,
44 Edwards, J.S., Gkinis, V., 2014. An ice core record of near-synchronous global
45 climate changes at the Bølling transition. *Nat. Geosci.* 7, 459–463.
46 doi:10.1038/ngeo2147

- 1 Sander, R., 2015. Compilation of Henry's law constants (version 4.0) for water as
2 solvent. *Atmospheric Chem. Phys.* 15, 4399–4981. doi:10.5194/acp-15-4399-
3 2015
- 4 Schwander, J., Barnola, J.M., Andrié, C., Leuenberger, M., Ludin, A., Raynaud, D.,
5 Stauffer, B., 1993. The age of the air in the firn and the ice at Summit, Greenland.
6 *J. Geophys. Res.* 98, 2831–2838. doi:10.1029/92jd02383
- 7 Schwander, J., Sowers, T., Barnola, J.M., Blunier, T., Fuchs, A., Malaizé, B., 1997. Age
8 scale of the air in the summit ice: Implication for glacial-interglacial temperature
9 change. *J. Geophys. Res.* 102, 19483–19493. doi:10.1029/97jd01309
- 10 Severinghaus, J.P., Albert, M.R., Courville, Z.R., Fahnestock, M.A., Kawamura, K.,
11 Montzka, S.A., Mühle, J., Scambos, T.A., Shields, E., Shuman, C.A., Suwa, M.,
12 Tans, P., Weiss, R.F., 2010. Deep air convection in the firn at a zero-accumulation
13 site, central Antarctica. *Earth Planet. Sci. Lett.* 293, 359–367.
14 doi:10.1016/j.epsl.2010.03.003
- 15 Sigl, M., Winstrup, M., McConnell, J.R., Welten, K.C., Plunkett, G., Ludlow, F.,
16 Büntgen, U., Caffee, M., Chellman, N., Dahl-Jensen, D., Fischer, H., Kipfstuhl,
17 S., Kostick, C., Maselli, O.J., Mekhaldi, F., Mulvaney, R., Muscheler, R.,
18 Pasteris, D.R., Pilcher, J.R., Salzer, M., Schüpbach, S., Steffensen, J.P., Vinther,
19 B.M., Woodruff, T.E., 2015. Timing and climate forcing of volcanic eruptions for
20 the past 2,500 years. *Nature* 523, 543–549. doi:10.1038/nature14565
- 21 Sowers, T., Bender, M., Raynaud, D., Korotkevich, Y.S., 1992. $\delta^{15}\text{N}$ of N_2 in air trapped
22 in polar ice: A tracer of gas transport in the firn and a possible constraint on ice
23 age-gas age differences. *J. Geophys. Res. Atmospheres* 97, 15683–15697.
24 doi:10.1029/92JD01297
- 25 Spahni, R., Schwander, J., Fluckiger, J., Stauffer, B., Chappellaz, J., Raynaud, D., 2003.
26 The attenuation of fast atmospheric CH_4 variations recorded in polar ice cores.
27 *Geophys. Res. Lett.* 30, 1571. doi:10.1029/2003gl017093
- 28 Stowasser, C., Buizert, C., Gkinis, V., Chappellaz, J., Schüpbach, S., Bigler, M., Faïn, X.,
29 Sperlich, P., Baumgartner, M., Schilt, A., Blunier, T., 2012. Continuous
30 measurements of methane mixing ratios from ice cores. *Atmospheric Meas. Tech.*
31 5, 999–1013. doi:10.5194/amt-5-999-2012
- 32 Sturrock, G.A., Etheridge, D.M., Trudinger, C.M., Fraser, P.J., Smith, A.M., 2002.
33 Atmospheric histories of halocarbons from analysis of Antarctic firn air: Major
34 Montreal Protocol species. *J. Geophys. Res. Atmospheres* 107, 4765.
35 doi:10.1029/2002JD002548
- 36 Trudinger, C.M., Enting, I.G., Etheridge, D.M., Francey, R.J., Levchenko, V.A., Steele,
37 L.P., Raynaud, D., Arnaud, L., 1997. Modeling air movement and bubble trapping
38 in firn. *J. Geophys. Res. Atmospheres* 102, 6747–6763. doi:10.1029/96JD03382
- 39 Weiler, K., 2008. On the composition of firn air and its dependence on seasonally varying
40 atmospheric boundary conditions and the firn structure. PhD thesis, University of
41 Bern, Bern, Switzerland.

42

- 1 Table 1. Locations, site characteristics and other relevant information for ice cores
 2 featured in this study. Please refer to footnotes for explanation of abbreviations.

Ice core & location (see map Fig. S1)	Depth interval (m)	Gas age interval (yrAD)	Δ age and FWHM (yr)	Accum. rate (cm ice yr ⁻¹)	Mean annual temp. (°C)	Mean liq. cond. (μS)	Age scale
B40 Drønning Maud Land, E. Antarctica 75.001°S, 0.068°E 2911 m elevation	200–88	331– 1710	811 65	6.8 ^b	-46 ^b	1.33	Ice: ALC+VS Gas: tied to WDC06A-7 ^f
D4 S. Central Greenland 71.40°N, 43.08°W 2,713 m elevation	146–61	1825– 1961	90 14	41	-24	101	Ice: ALC+VS Gas: tied to WDC06A-7 ^f & Law Dome ^g
NEEM NW Greenland 77.45°N, 51.06°W 2,450 m elevation	573–399	-682– 322	187 ^a 17	22 ^c	-28.9 ^e	122	Ice: GICC05 ^h Gas: GICC05 ^h
NGRIP Central Greenland 75.10°N, 42.32°W 2,917 m elevation	569–519	-929– 616	235 18	19 ^d	-31.5 ^d	122	Ice: GICC05 ^h Gas: tied to WDC06A-7 ^f
		254–207	980– 1237			105	
		108–74	1780– 1926			107	
Tunu13 NE Greenland 78.035°N, 33.879°W 2,200 m elevation	213–73	836– 1893	314–369 21–27	10–14	-29 ^e	115	Ice: ALC+VS ⁱ Gas: tied to WDC06A-7 ^f
WAIS Divide West Antarctica 79.47°S, 112.08°W 1766 m elevation	n/a	n/a	208 ^j	20 ^j	-31 ^j	n/a	n/a

3 Footnotes:

4 Δ age = difference between gas age and ice age. If no reference is provided, value is estimated by age scale
 5 synchronisation or OSU firm air model.

6 FWHM= Full Width at Half Maximum of gas age distribution at close-off depth estimated by OSU firm air
 7 model (Rosen et al., 2014).

8 Mean liq. cond. = mean liquid conductivity value for ice core analysed

9 ALC=annual layer count; VS=volcanic synchronisation

10 Gas age scales do not incorporate lock-in zone measurements.

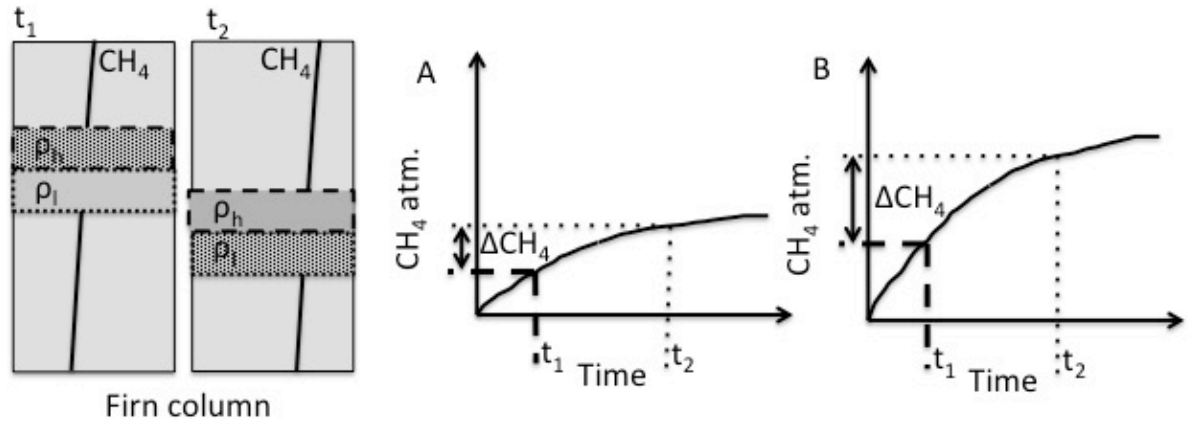
11 References:

12 a=(Buizert et al., 2014); b=(Klein, 2014); c=(NEEM community members, 2013); d=(NGRIP community
 13 members, 2004); e=(Butler et al., 1999); f=(Mitchell et al., 2013); g=(MacFarling Meure et al., 2006);
 14 h=(Rasmussen et al., 2013); i=(Sigl et al., 2015); j=(Mitchell et al., 2011)

1 Table 2. Discrete CH₄ and total air content measurements on Tunu13 samples containing
 2 melt layers. Estimated CH₄ concentrations of the melt layers result from a simple mixing
 3 calculation using air content measurements made on Summit melt layer samples. Values
 4 in parentheses reflect the range of melt layer air content values measured. Predicted CH₄
 5 values are calculated using the assumption that the melt layer was in equilibrium with the
 6 atmosphere, according to Henry's Law (0°C, 0.750 atm.). Henry's Law constants for
 7 CH₄, O₂ and N₂ were obtained from NIST Chemistry WebBook (webbook.nist.gov).
 8 CH₄ concentrations of adjacent samples are used as atmospheric concentrations at time of
 9 melt layer formation. All of these samples are from the Tunu13 Main core.

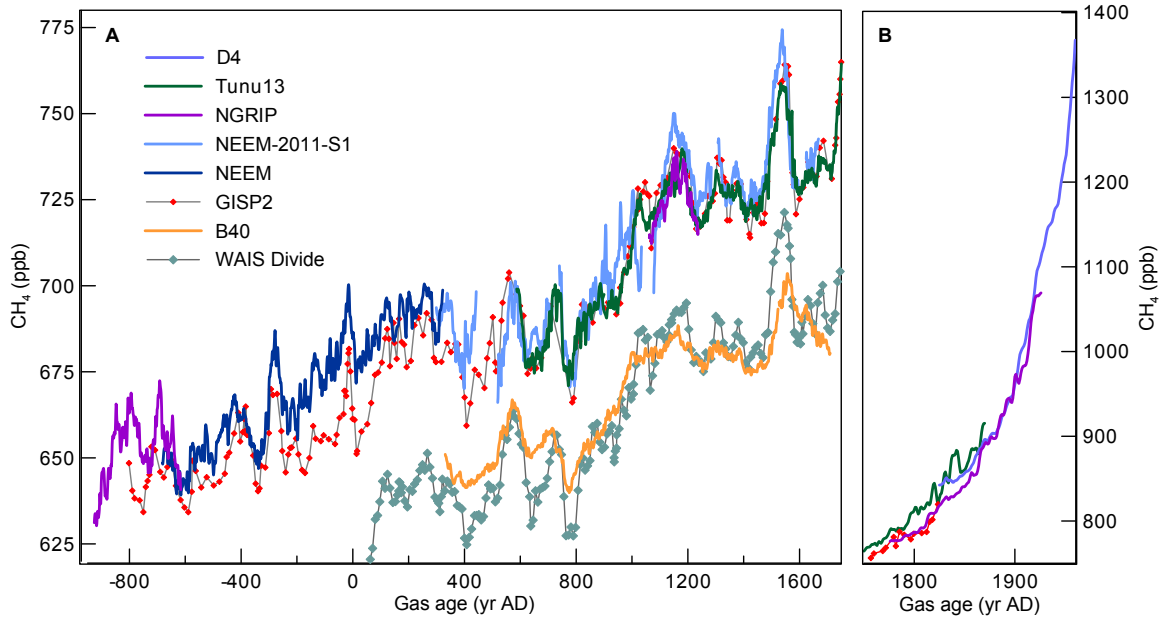
Sample depth range (m)	Sample CH ₄ conc. (ppb)	Sample total air content (cm ³ /g ice STP)	Melt layer thickness (mm)	Estimated CH ₄ conc. of melt layer (ppb)	x-fold CH ₄ enrichment of ML relative to sample	Mean CH ₄ conc. of adjacent samples (ppb)	Predicted CH ₄ conc. of melt layer in equilib. with atmos. (ppb)
113.910–113.970	773.6	0.0956	4.0	6355 (4781–9940)	8.6	737.1	1492
153.225–153.300	730.3	0.0859	4.0	1829 (1519–2533)	2.5	723.9	1465
156.235–156.285	744.1	0.0941	4.0	5356 (4076–8356)	7.4	721.0	1460
181.710–181.760	700.3	0.0970	4.0	2539 (2020–3721)	3.7	686.1	1389
194.610–194.700	771.9	0.0847	24.0	3683 (2842–5596)	5.4	684.0	1385

10



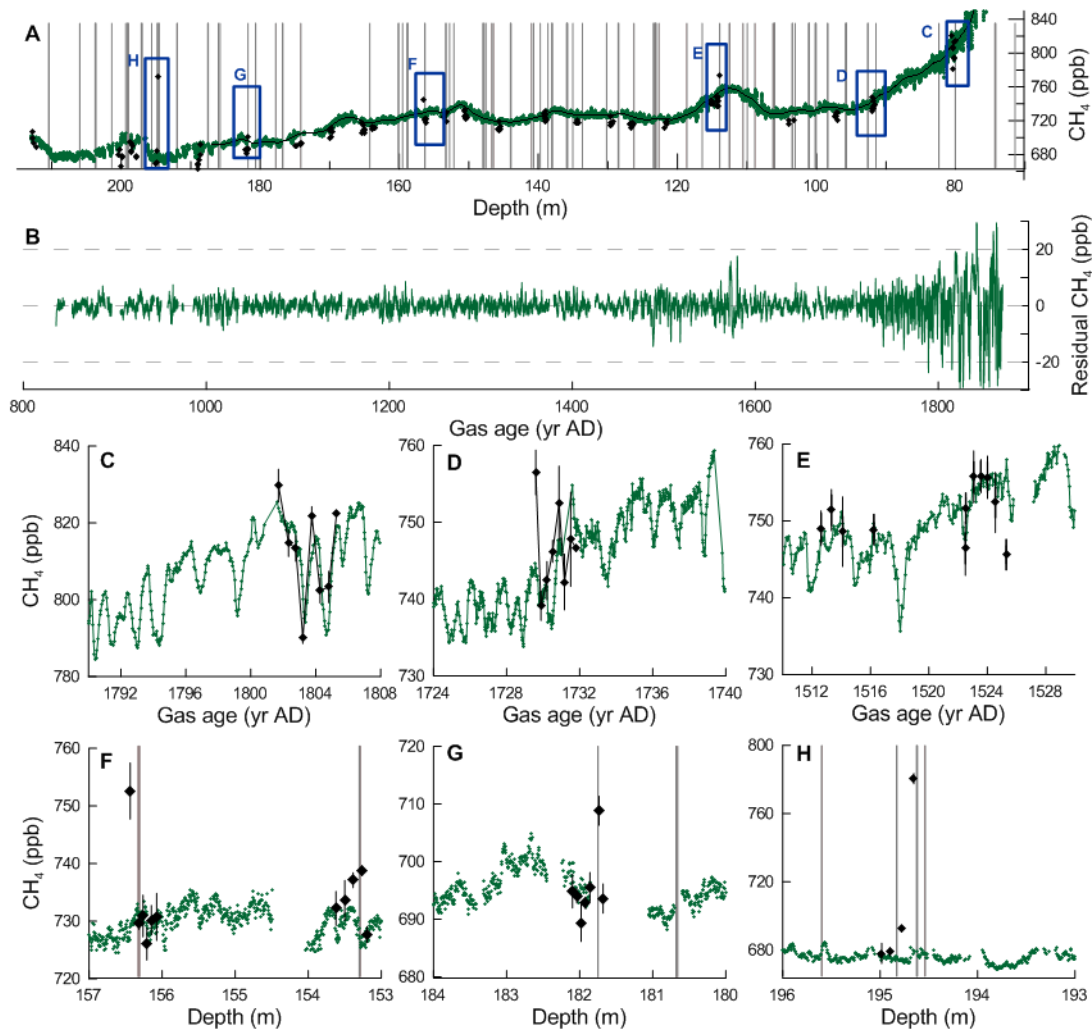
1
 2 Figure 1.: Schematic to illustrate how the layered bubble trapping mechanism can
 3 generate high frequency CH₄ artifacts in ice cores. At time t₁, air bubbles within the
 4 relatively high density (ρ_h) layer are closed off at a relatively shallow depth in the firn
 5 column. At time t₂, air bubbles with the relatively low density (ρ_l) layer are closed off
 6 deeper in the firn column. Between t₁ and t₂ the atmospheric concentration of CH₄ is
 7 increasing and so the CH₄ concentration in the diffusive column also increases,
 8 generating a CH₄ concentration difference ΔCH₄ between the bubbles in depth-adjacent
 9 layers trapped at t₁ and t₂. Increasing the atmospheric CH₄ growth rate (B compared to
 10 A) results in a larger ΔCH₄. A negative atmospheric growth rate would cause a change in
 11 the sign of ΔCH₄.

1



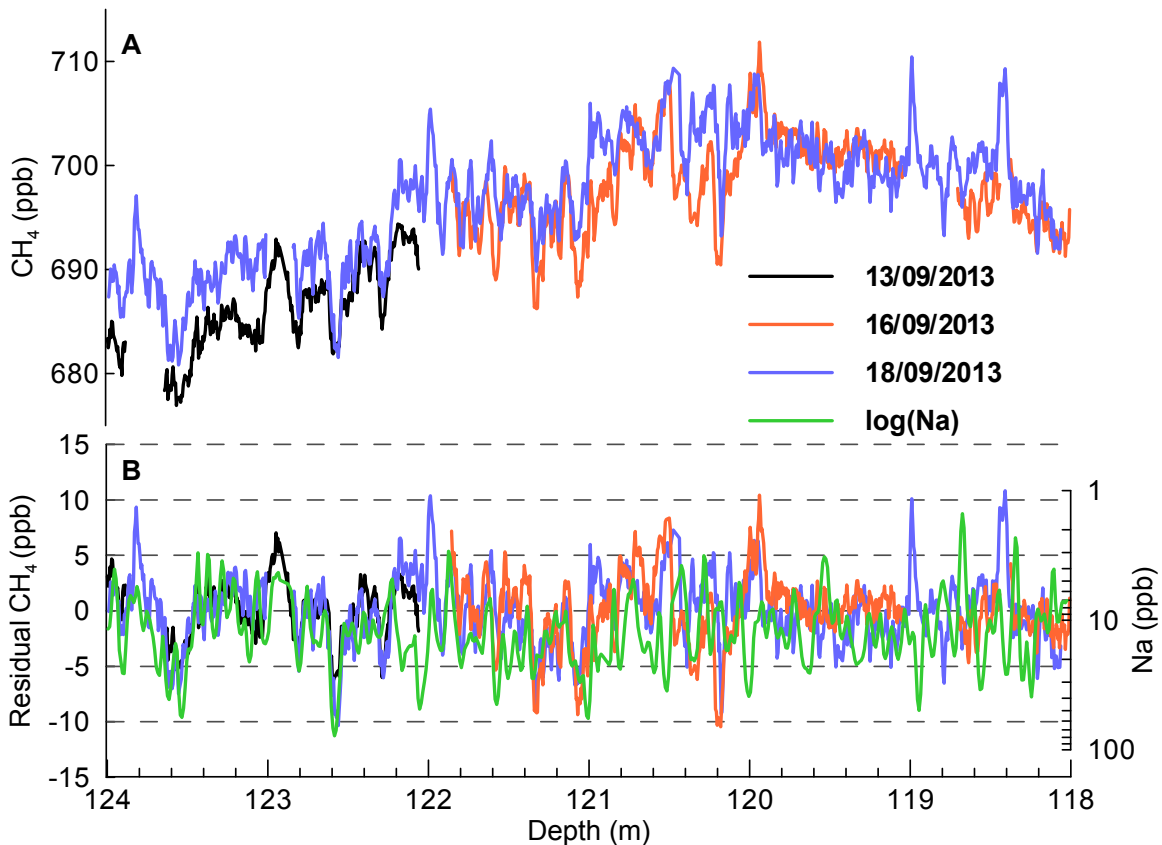
2

3 Figure 2. Late Holocene continuous CH₄ data from Tunu13, D4, NGRIP and NEEM
4 Greenland ice cores and B40 Antarctic ice core for time periods -900–1750 AD (A) and
5 1750–1960 AD (B). Each record is a cubic spline fit with 1 yr sample spacing to the 5 s
6 integrated data. No data from the lock-in zone are included on this figure. Also plotted
7 are discrete CH₄ data from GISP2 and WAIS Divide ice cores (Mitchell et al., 2013) and
8 NEEM-2011-S1 continuous CH₄ data (Rhodes et al., 2013).



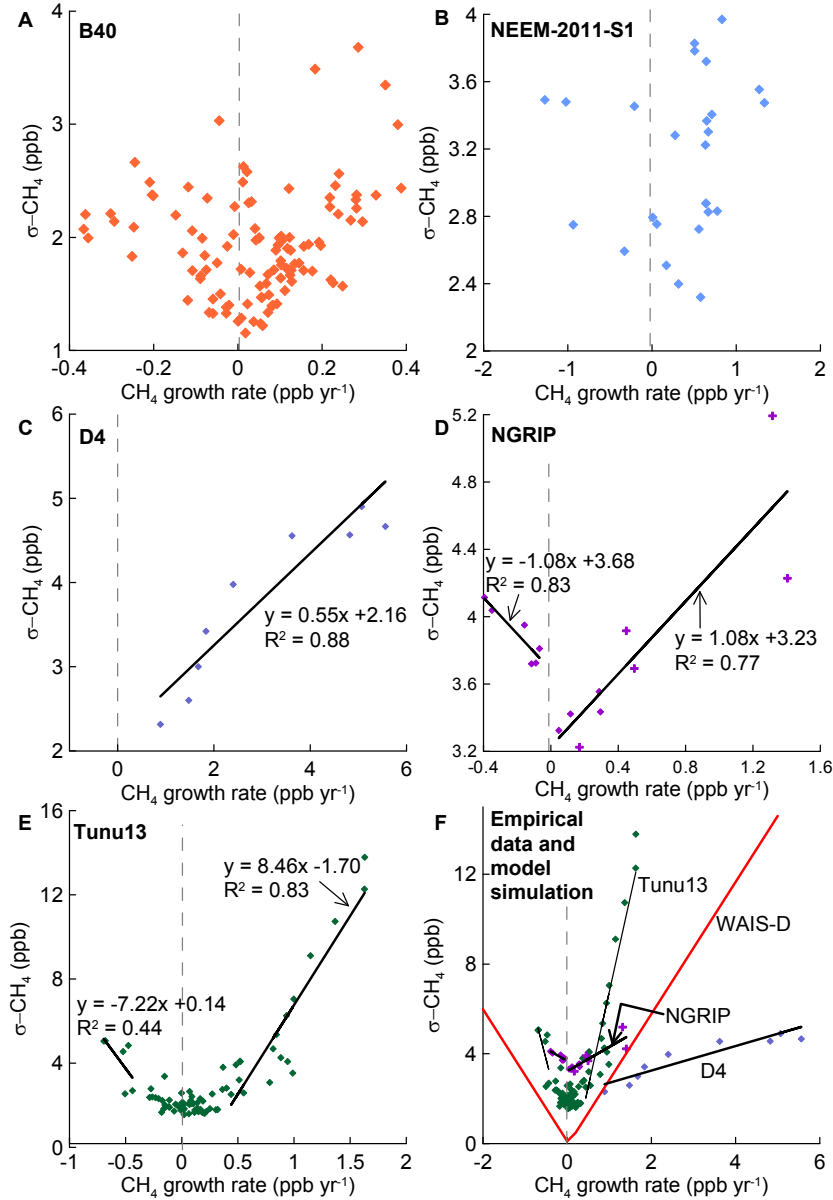
1
 2 Figure 3. Decimetre-scale CH₄ variability in Tunu13 mature ice captured by continuous
 3 (green) and discrete (black diamonds) analyses: A) Both records on depth scale with
 4 vertical grey lines indicating depths of bubble-free layers observed; B) Residual high
 5 frequency non-atmospheric component of Tunu13 signal: continuous record from panel
 6 A (green) minus cubic spline fit (black line on panel A). Older data from below 172 m
 7 depth are excluded because there are too many data gaps resulting from poor core quality.
 8 Y-axis has been clipped at -30 and +30 ppb. Data minimum and maximum are -38 and
 9 36 ppb; C, D & E) Zoomed views of high frequency CH₄ variability within blue
 10 rectangles displayed on panel A; F, G & H) Zoomed views of anomalously high discrete
 11 CH₄ concentrations associated with melt layers. CH₄ concentrations of discrete data
 12 points are increased by 8.5 ppb on panels C-H to aid comparison with online data. 2 σ
 13 internal precision uncertainty bars are plotted for discrete data. Horizontal bars on

- 1 discrete measurements represent depth interval of each sample. Depth uncertainty for the
- 2 continuous data is estimated to be ± 2 cm (2σ).

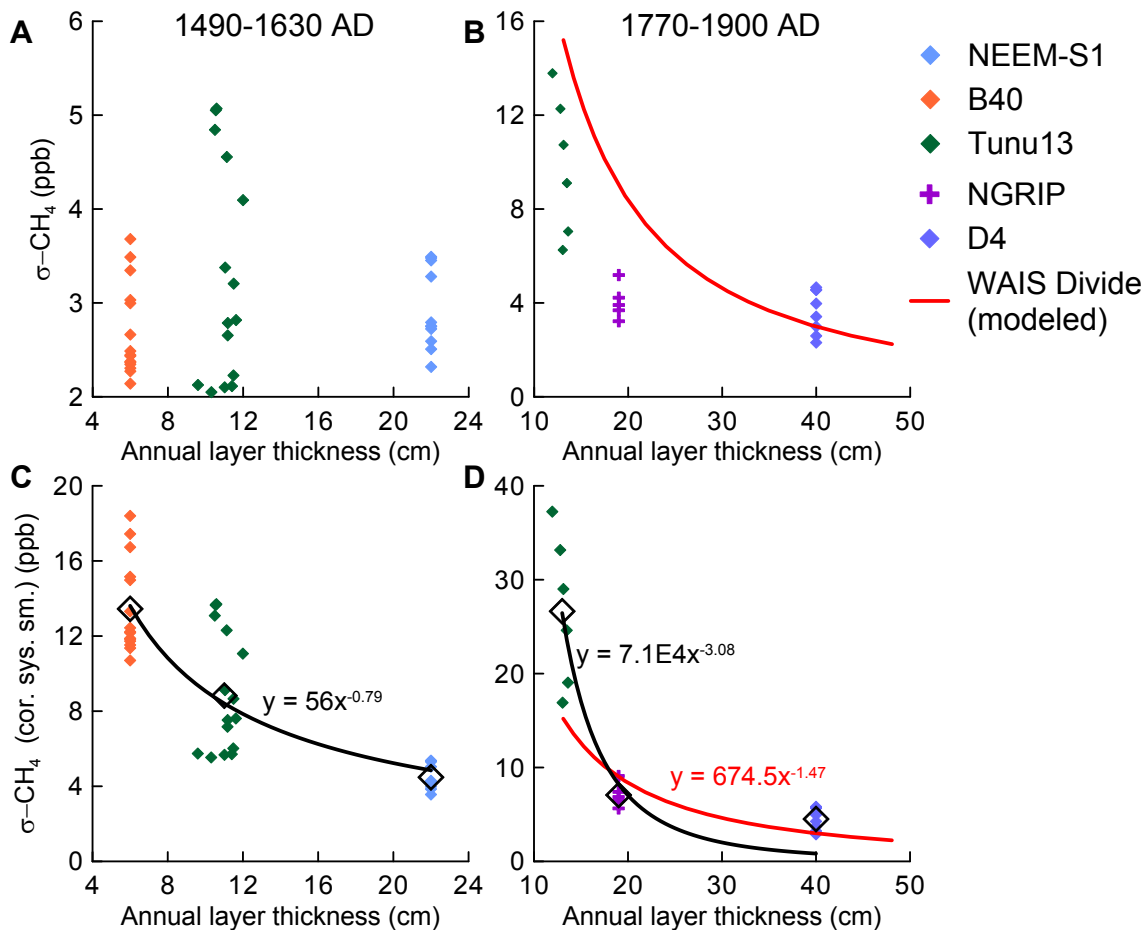


1

2 Figure 4. High frequency CH₄ variability in B40 (E. Antarctica) ice. Measured signals
 3 (A) and the residual (signal – spline fit) (B) are shown. Variability is replicated by
 4 analyses performed on the three dates displayed in legend (dd/mm/yyyy). Gas extraction
 5 was performed using a Membrana micromodule degasser on 13/09/2013 and an IDEX in-
 6 line degasser on 16/09/2013 and 18/09/2013 (Table S1). Although it is difficult to be
 7 certain that anomalously high CH₄ spikes are not the result of ambient air entry at the
 8 melterhead, the anomalously low troughs cannot be analytical artifacts. Also shown on
 9 panel B is Na concentration, which typically co-varies with Cl concentration. Many of
 10 the anomalously low CH₄ values are coincident in depth with relatively high Na. This
 11 depth interval is dated as 1493–1583 AD gas age.



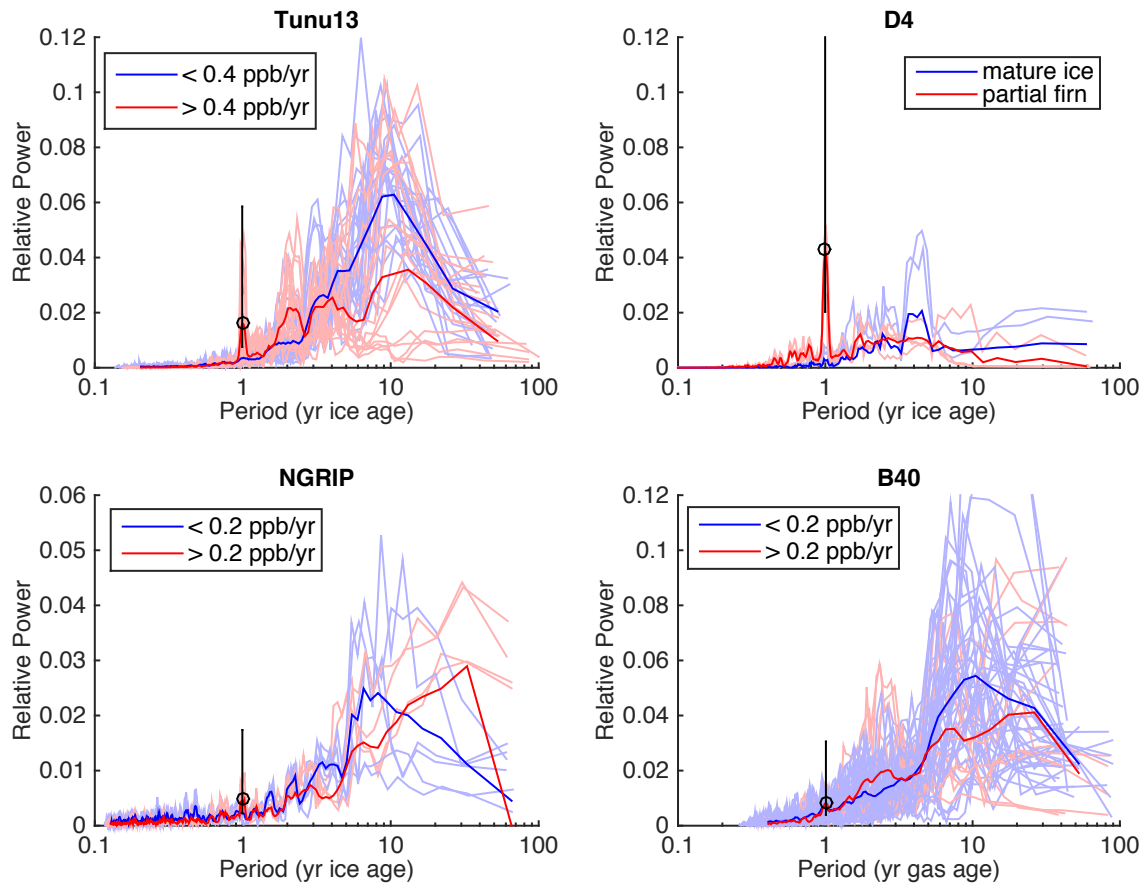
1
2 Figure 5. Relationship between CH₄ growth rate and high frequency CH₄ variability (σ-
3 CH₄) in the following ice cores: B40 (A), NEEM-2011-S1 (B), D4 (C), NGRIP (D),
4 Tunu13 (E). σ-CH₄ is calculated every 10 yr for intervals of 40 yr duration (except for 5
5 NGRIP data points (cross symbols), which are discrete 10 yr intervals with no overlap,
6 due to poor core quality and discontinuous record). Linear regression of growth rate and
7 σ-CH₄ is displayed where appropriate. A linear fit is applied to Tunu13 and D4 data with
8 growth rates > ± 0.4 ppb yr⁻¹ and to NGRIP data with growth rates > ± 0.1 ppb yr⁻¹.
9 Panel F displays data from Tunu13, D4 and NGRIP with firm air transport model output
10 for the WAIS Divide ice core.



1

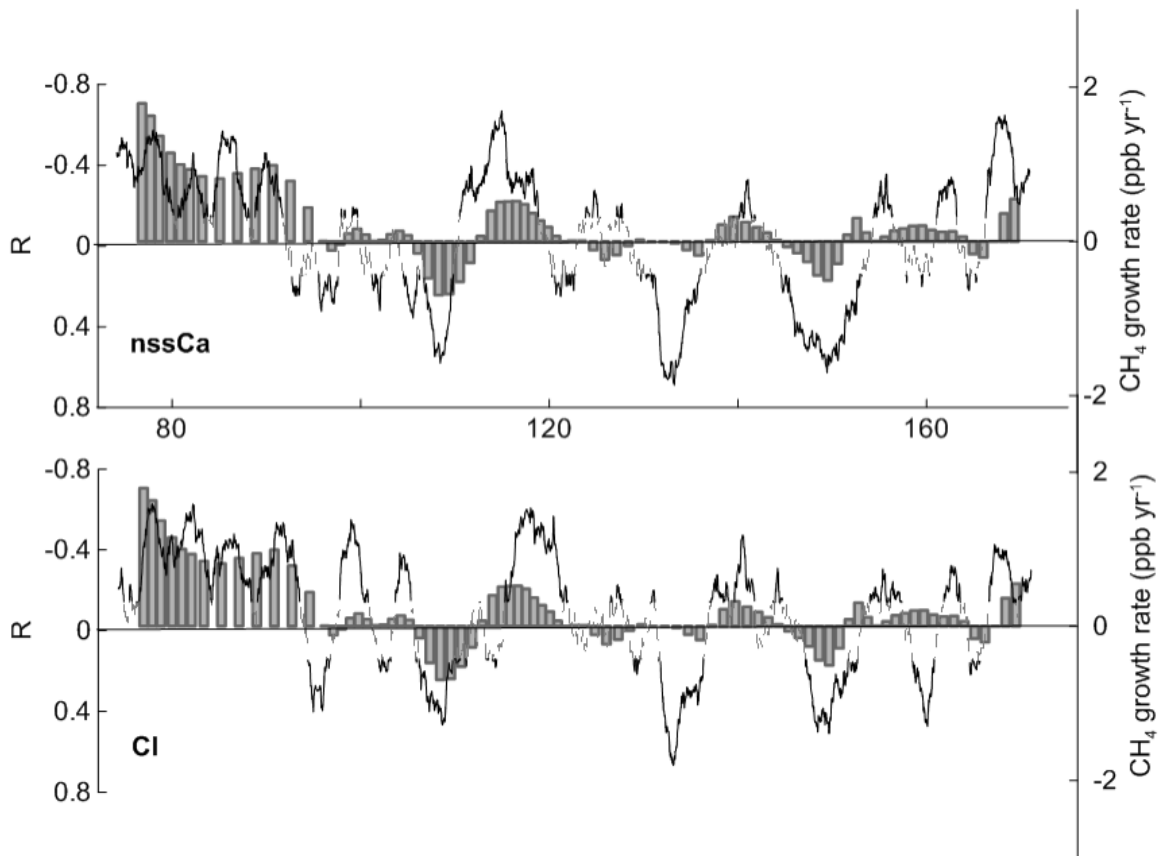
2 Figure 6. Relationship between accumulation rate and high frequency CH₄ variability.
 3 The vertical panels represent two time intervals: 1490–1630 AD (A) and 1770–1900 AD
 4 (B) for which high resolution CH₄ data are available from three ice cores with different
 5 accumulation rates. Note that the three clusters of data points for each time period do not
 6 represent the same ice cores in each case. The top row (A & B) displays CH₄ standard
 7 deviation (σ) about the long-term spline. Values are calculated every 10 yr for intervals
 8 of 40 yr duration as Fig. 5 (except for NGRIP data points on B&D that represent discrete
 9 10 yr intervals). The bottom row (C & D) displays $\sigma\text{-CH}_4$ values adjusted (increased by
 10 1.25–5 depending on ice core) to correct for the damping effect of the continuous
 11 analytical system (Fig. S2). Mean values for each ice core on each panel are displayed
 12 (black diamonds) with power law relationships (black line). Also shown is the
 13 relationship between accumulation rate and $\sigma\text{-CH}_4$ for WAIS Divide (at 2.5 ppb yr⁻¹
 14 atmospheric growth rate) as predicted by the CIC firm air transport model.

15



1
2
3
4
5
6
7
8
9
10
11
12
13
14

Figure 7. Multi-taper method (MTM) spectra of high frequency, non-atmospheric residual CH_4 variability of four ice cores. MTM was performed in the ice age domain using 2 tapers and 3 degrees of freedom. Each spectrum represents a 40 yr window of data. For Tunu13, NGRIP and B40 each spectrum is colour-coded according to the CH_4 growth rate of that data window. For D4, spectra are colour-coded according to whether or not the time window encompasses data from the lock-in zone (< 82 m depth). All D4 spectra represent time windows of CH_4 growth rate $> 0.4 \text{ ppb yr}^{-1}$. The bold lines represent averaged spectra for the low/high growth rate or mature ice/partial firn categories. Black open circles represent the mean relative power at 1 yr period. Vertical lines represent 90% confidence intervals for the averaged spectra (bold, red lines only) based on a chi-squared distribution. Spectral peaks are significant for Tunu13 and D4 because the confidence interval exceeds the background spectral noise.



1
 2 Figure 8. Moving window Spearman's rank correlation between concentrations of non-
 3 sea salt (nss) Ca and Cl and σ -CH₄ in the Tunu13 ice core (line) compared to CH₄ growth
 4 rate (vertical bars). Note the reverse direction of the left-hand y-axes. Significant ($p <$
 5 0.05) (solid line) and non-significant (grey dashed line) coefficient of correlation (R)
 6 values are plotted. Correlation is calculated for non-overlapping, 2 m length windows
 7 (using 0.5–5 m length windows produces similar results). The σ -CH₄ time series is
 8 resampled to the depth spacing of chemistry data (1 cm) so $n = 200$ for each window.